MATHEMATICAL MODELING OF BINARY INTERPHASE DIFFUSION IN GAS-EXPANDED LIQUIDS

by
Gülçin Cem

Submitted to the Institute of Graduate Studies in
Science and Engineering in partial fulfillment of
the requirements for the degree of
Master of Science
in
Chemical Engineering

Yeditepe University
2011

MATHEMATICAL MODELING OF BINARY INTERPHASE DIFFUSION IN GAS-EXPANDED LIQUIDS

APPROVED BY:

Assist. Prof. Betül Ünlüsü (Advisor) .....

Assist. Prof. Çerağ Dilek .....

Assist. Prof. Özlem Güçlü Üstündağ .....

DATE OF APPROVAL: .../.../....

ACKNOWLEDGMENTS

First and foremost I would like to thank my advisor Assist. Prof. Betül Ünlüsü, for her guidance and advices throughout the research and for her patience and help during preparation of this thesis.

I would like to thank Binnaz Coşkunkan, Melek Şekerci, Merve Yüksel, Hatice Semizer, Zeynep Çapanoğlu, Gökçe Üdenir and all other friends for the support they provided me through my entire life.

A very special thanks goes to Orçun Özeral without whose love and encouragement I would not have finished this thesis.

I am thankful to my beloved family whose endless support and love I felt all the time.

ABSTRACT

MATHEMATICAL MODELING OF BINARY INTERPHASE DIFFUSION IN GAS-EXPANDED LIQUIDS

In recent years, carbon dioxide-expanded liquids (CXLs) have emerged as promising media for performing catalytic reactions, separations and polymer processing. The addition of high pressure carbon dioxide to a system containing a liquid initiates two-way mass transfer. Carbon dioxide dissolves into the liquid and the liquid diffuses into carbon dioxide. Yet, the phase interface is not stationary because the mass transfer from liquid to vapor is not equal to that from vapor to liquid. The aim of the present work is to investigate binary interphase diffusion in CXL systems as a variation of the Stefan problem, two phases separated by a moving boundary. The model equations incorporate two partial differential equations describing the diffusion of the species in each phase and an ordinary differential equation accounting for the movement of the interface. Numerical solution codes based on a fixed-grid finite difference formulation are developed to solve them. The diffusion coefficients are estimated using the Maxwell-Stefan approach which splits Fick Diffusivity into two terms: Drag effects and thermodynamic effects. Maxwell-Stefan diffusivities account for the frictional drag applied by species on one another during the diffusion. Thermodynamic correction factor is expressed in terms of the derivative of fugacity coefficients with respect to composition at high pressure. The diffusion in two different ionic liquids-carbon dioxide systems, [bmim][PF_6]-CO_2 and [thdp][Cl]-CO_2, and methanol-carbon dioxide system is examined. Phase interface displacements, composition profiles and the effects of using pressure-corrected infinite dilution diffusivities and composition-dependent Fick diffusivities on the interface displacements are presented.

ÖZET

GAZLA GENLEŞMİŞ SIVILARDA FAZLAR ARASI İKİLİ DİFÜZYONUN MATEMATİKSEL MODELLENMESİ

Karbondioksit ile genleşmiş sıvılar, katalitik reaksiyonlar, ayrıştırma ve polimer işlemelerinin gerçekleştirilebileceği gelecek vaat eden ortamlar olarak son yıllarda öne çıkmışlardır. Sıvı içeren bir sisteme yüksek basınçlı karbondioksit eklenmesi çift yönlü kütle aktarımını başlatır. Karbondioksit sıvının içinde çözünürken, sıvı da karbondioksit fazında yayınır. Ancak, faz ara-yüzeyi durağan değildir, çünkü sıvıdan gaza olan kütle transferi, gazdan sıvıya olan kütle transferine eşit değildir. Bu çalışmanın amacı karbondioksitle genleşmiş sıvı sistemlerinde fazlar arası ikili difüzyonu, bir Stefan problemi çerçevesinde (hareketli sınır ile ayrılmış iki faz olarak) incelemektir. Model denklemleri, maddelerin her fazdaki difüzyonunu tanımlayan iki kısmi diferansiyel denklem ile ara yüzey hareketini ifade eden bayağı diferansiyel denklemi içerir. Bu denklemleri çözmek için sabit aralıklı sonlu farklar yöntemine dayanan hesapsal çözüm programları geliştirilmiştir. Difüzyon katsayıları, Fick katsayılarını, çekme etkileri ve termodinamik etkiler olarak ikiye ayıran Maxwell-Stefan yaklaşımı ile hesaplanmıştır. Maxwell-Stefan difüzyon katsayıları, difüzyon sırasında maddelerin birbirine uyguladığı sürtünme çekmesini açıklar. Termodinamik düzeltme faktörü ise yüksek basınçta fugasite katsayılarının kompozisyona göre türevi ile ifade edilir. İki farklı iyonik sıvı-karbondioksit sistemi, [bmim][PF_6]-CO_2 ve [thdp][Cl]-CO_2, ve methanol-karbondioksit sistemindeki difüzyon incelenmiştir. Faz ara-yüzeyinin konumundaki değişim, kompozisyon profilleri ve basınca göre düzeltilmiş sonsuz seyreltimdeki difüzyon katsayıları ile kompozisyona bağlı Fick difüzyon katsayılarının kullanılmasının ara-yüzeyin yer değiştirmesine etkileri sunulmuştur.

TABLE OF CONTENTS

ACKNOWLEDGMENTS iii
ABSTRACT iv
ÖZET v
TABLE OF CONTENTS vi
LIST OF FIGURES viii
LIST OF TABLES xi
LIST OF SYMBOLS / ABBREVIATIONS xii
1. INTRODUCTION 1
2. THEORETICAL BACKGROUND I: FUNDAMENTALS AND APPLICATIONS OF SUPERCRITICAL FLUIDS AND GAS EXPANDED LIQUIDS 3
2.1. SUPERCRITICAL FLUIDS 3
2.1.1. Supercritic CO_2 As A Solvent Media 5
2.1.2. Supercritical Drying 6
2.1.3. Aerogels 7
2.1.4. Sol Gel Process Steps 9
2.2. GAS EXPANDED LIQUIDS 11
2.2.1. Carbondioxide Expanded Liquids 12
2.2.2. Applications Of Gas Expanded Liquids 13
2.3. IONIC LIQUIDS 16
2.3.1. Applications of Ionic Liquids 16
2.3.2. High Pressure Phase Behaviour of Ionic Liquid-CO_2 Systems 17
2.3.2.1. The [bmim][PF_6]-CO_2 System 18
2.3.2.1. The Other Ionic Liquids-CO_2 System 18
3. THEORETICAL BACKGROUND II: DIFFUSION AND NUMERICAL TREATMENT OF THE DIFFUSIONAL PROCESS INVOLVING A MOVING INTERFACE 19
3.1. DIFFUSION 19
3.1.1. Fick's Fist Law of Diffusion 19
3.1.2. Diffusion in Binary Mixtures 20
3.2. NUMERICAL TREATMENT OF THE MOVING INTERFACE 24

3.2.1. The Movable Grid Method 24
3.2.2. The Fixed Grid Method 25
4. THEORETICAL BACKGROUND III: THERMODYNAMIC MODELING OF PHASE EQUILIRIUM 30
4.1. BASIC THERMODYNAMICS OF PHASE EQUILIBRIUM 30
4.2. EQUATIONS OF STATE 32
4.3. MIXING-COMBINING RULES 35
5. DEVELOPMENT OF THE MODEL 39
6. RESULTS AND DISCUSSION 45
6.1. CONVERGENCE OF THE NUMERICAL METHOD 45
6.2. COMPARISON WITH LITERATURE DATA 46
6.3. INTERPHASE DIFFUSION IN CARBON DIOXIDE-EXPANDED LIQUIDS 47
6.3.1. Carbon Dioxide-Ionic Liquid Systems At High Pressure 48
6.3.2. Carbon Dioxide-Methanol System At High Pressure 52
7. CONCLUSIONS AND FUTURE WORK 58
APPENDIX A : FLOWCHARTS OF FORTRAN PROGRAMS USED 60
APPENDIX B : VISCOSITY DATA 62
APPENDIX C : ESTIMATED PARAMETERS FOR METHANOL-CO_2 SYSTEM 63
REFERENCES 65

LIST OF FIGURES

Figure 2.1. Phase diagram of a pure substance 3

Figure 2.2. Phase behaviour of CO_2 5

Figure 2.3. CO_2 becoming a SCF 5

Figure 2.4. Differences between drying methods 7

Figure 2.5. Samples dried by supercritical drying and air drying..... 8

Figure 2.6. Superinsulating property of silica aerogel 9

Figure 2.7. Formation of aerogel and xerogel 10

Figure 2.8. Vapor-liquid equilibrium of methanol and CO_2 at 40° C 13

Figure 2.9. Phase behaviour of IL, [bmim][PF_6] with CO_2 at 40° C 13

Figure 3.1. Illustration of Fick's first law 20

Figure 3.2. Control Volume 21

Figure 3.3. Murray and Landis Variable Grid 25

Figure 3.4. Elements of fixed grid method 26

Figure 5.1. The prototype system I 39

Figure 5.2. The prototype system II 40

Figure 6.1. Numerical results at different time steps for methanol-CO_2 system at 73.9 bar, 313.14 K 46

Figure 6.2. Numerical results at different grid sizes for methanol-CO_2 system at 73.9 bar, 313.14 K 46

Figure 6.3. Comparing experimental data and numerical results for methanol-air system at ambient pressure 47

Figure 6.4. Interface Displacement of [bmim][PF_6]-CO_2 system at 75 bars and 313.14 K 48

Figure 6.5. Composition profiles of [bmim][PF_6]-CO_2 system at t=2500 s 49

Figure 6.6. Average Mole fraction of CO_2 in liquid phase in [bmim][PF_6]-CO_2 system for t=2500 s 49

Figure 6.7. Interface Displacement of [thtdp][Cl]-CO_2 system at 75 bars and 313.14 K 50

Figure 6.8. Composition profiles of [thtdp][Cl]-CO_2 system at t=2500 s 51

Figure 6.9. Average Mole fraction of CO_2 in liquid phase in [thtdp][Cl]-CO_2 system for t=2500 s 51

Figure 6.10. Interface Displacement of Methanol-CO_2 system at 73.9 bars and 313.14 K 52

Figure 6.11. Composition profiles of Methanol-CO_2 system at t=2500 s 53

Figure 6.12. Average Mole fraction of CO_2 in liquid phase in Methanol-CO_2 system for t=2500 s 53

Figure 6.13. Change in Maxwell-Stefan diffusity of Methanol-CO_2 system at 73.9 bars and 313.14 K 54

Figure 6.14. Change in thermodynamic factor of Methanol-CO_2 system at 73.9 bars and 313.14 K 55

Figure 6.15. Change in Fick diffusivity of Methanol-CO_2 system at 73.9 bars and 313.14 K 55

Figure 6.16. Interface Displacement of Methanol-CO_2 system at 73.9 bars and 313.14 K with Fick Diffusivities 56

Figure 6.17. Interface Displacement of Methanol-CO_2 system at 73.9 bars and 313.14 K with evaporation and without evaporation 56

Figure A.1. Flowchart of the main program 60

Figure A.2. Flowchart of the subroutine ‘Diffusivity’ 61

Figure C.1. Calculated and experimental vapor mole fractions for Methanol-CO_2 system 64

Figure C.2. Calculated and experimental pressures for Methanol-CO_2 system 64

LIST OF TABLES

Table 2.1. Substances useful as supercritical fluids 4

Table 5.1. Infinite Dilution Diffusivities 44

Table 5.2. Maxwell-Stefan and Fick Diffusivities for Methanol-CO_2 system at 73.9 bar and 313.14 K 44

Table 6.1. Equilibrium mole fractions of CO_2 and [bmim][PF_6] at 313.15 K and 75 bar 50

Table 6.2. Equilibrium mole fractions of CO_2 and [thtdp][Cl] at 313.15 K and 75 bar 52

Table 6.3. Equilibrium mole fractions of CO_2 and methanol at 313.14 K and 73.9 bar 54

Table B.1. Viscosity of methanol at high pressure 62

Table B.2. Viscosity of [bmim][PF_6] at high pressure 62

Table C.1. Estimated Parameters for Methanol-CO_2 System at 313.14 K 63

LIST OF SYMBOLS

a	Empirical constant of temperature
b	Empirical constant of volume
$[B]$	Matrix of the dragg effects
C	Concentration
c_i	Concentration of species i
C_i^j	Concentration at i th grid and j th step
c_t	Total concentration
$[D]$	Matrix of the Fick diffusivities
D	Diffusion coefficient
Đ	Maxwell-Stefan diffusion coefficient
D_i	Diffusion coefficient of species i
D^0	Infinite dilution diffusivity
$\underline{G}^I$	Molar Gibbs energy of the phase
J	Diffusion flux
J_i	Diffusion flux of species i
$J^{R/L}$	Diffusional flux at the interface on the vapor side
$J^{L/R}$	Diffusional flux at the interface on the liquid side
Δm	Amount of global mass change
N_i	Molar flux of species i
N_t	Total molar flux
p	Fractional interface parameter
P_c	Critical pressure
p_i	Partial pressure of component i
R	Ideal gas constant
T	Temperature
T_c	Critical temperature
t	Time
u	Molar everage velocity
u_i	Molar average velocity of species i

V	Total volume
V_m	Molar volume
v^L	Velocity of liquid phase
v^V	Velocity of vapor phase
x	Mole fraction in liquid phase
x_i	Composition of species i
∇x_i	Composition gradient
y	Mole fraction in vapor phase
Z	Compressibility factor
α_{12}, α_{21}	Non-ramdomness parameter
$\alpha(T)$	Temperature dependence term
Γ	Thermodynamic correction factor
γ_1	Energy coefficient
η	Viscosity
κ	Parameter for Peng-Robinson equation of state
κ_1	Species-specific constant
μ_1	Chemical potential of species 1
ξ	Movement of the interface
φ_i	Fugacity coefficient of species i
ω	Acentric factor
[bmim][PF_6]	1-Butyl-3-methylimidazolium hexafluorophosphate
CXL	Carbondioxide expanded liquid
EOS	Equation of State
GXL	Gas expanded liquid
IL	Ionic liquid
SCF	Supercritical fluid
[thtdp][Cl]	Trihexyltetradecylphosphonium chloride

1. INTRODUCTION

Supercritical fluids are very dense gases with many properties superior to liquids or solvents. While there are many fluids that can be used in their supercritical state, carbon dioxide (CO_2) is the one most often used because it is considered environmentally friendly in comparison to strong solvents, and its critical temperature point and operating pressures are relatively easy to work with [1].

Supercritical CO_2 and its associated technologies are being used in many applications, as extraction, reaction and solvent regeneration, to replace hazardous solvents, lower costs, and improve efficiencies. It should be noted that while supercritical CO_2 is excellent for dissolving small, non-polar organic compounds, it is less effective in dissolving many polar or ionic compounds and large polymers (except for fluorinated oligomers).

Gas-expanded liquids (GXLs) are an environmentally-benign class of solvent systems suitable for reactions and separations. GXLs are liquid mixtures consisting of an organic solvent combined with a high-fluidity gas, such as CO_2, in the near-critical regime. Carbon dioxide-expanded liquids (CXLs) are divided into three classes. The members of the first class (Class 1) such as water have insufficient ability to dissolve CO_2. The second class (Class 2) including liquids such as methanol, hexane and most other traditional organic solvents, dissolve large amounts CO_2. The third class (Class 3) includes liquids such as ionic liquids, liquid polymers, which dissolve only moderate amounts of CO_2 [2].

The aim of the present work is to investigate the dissolution of carbon dioxide in two ionic liquids ([bmim][PF_6] and [thdp][Cl]) and methanol at high pressure. The primary model used is the Fick's Law in one-dimensional form. Because a significant amount of mass is transferred in these systems, the phase-interface does not stay stationary. The change in the position of the interface is taken into account as an ordinary differential equation. The equations governing the diffusion of species and the movement of the phase-interface are solved using a numerical solution technique based on a fixed-grid finite

difference formulation. The interface displacements and composition profiles during the dissolution process in the aforementioned systems are examined.

In methanol-carbon dioxide system, the effect of using composition-dependent diffusivities on the interface displacements is also investigated. The composition-dependent Fick diffusivity is calculated based on the Maxwell-Stefan formulation. In this approach, Fick Diffusivity is the product of the Maxwell-Stefan diffusivity and the thermodynamic correction factor which is estimated using the Peng Robinson Equation of State with Stryjek-Vera modification and Wong-Sandler mixing rules.

Peng-Robinson equation of state is a simple but powerful cubic equation of state that is widely used in industry [3]. The temperature and acentric factor dependence of the Peng-Robinson equation of state have been modified by Stryjek and Vera [4], to allow the accurate reproduction of the vapor pressure data for a wide variety of substances. Wong-Sandler (WS) mixing rule produces the desired equation of state behavior at both low and high densities without being density dependent and allows extrapolation over wide ranges of temperature and pressure. The WS mixing rule can predict the vapor-liquid equilibria of highly nonideal mixtures [5].

Fundamentals of supercritical fluids, gas-expanded liquids and their applications are presented in Chapter 2. Diffusion and the numerical treatment of moving boundary problems are introduced in Chapter 3. Chapter 4 is to review the thermodynamic modeling of phase equilibrium. Chapter 5 elaborates on the development of model equations and determination of the model parameters. The results and discussions are presented in Chapter 6. Finally, Chapter 7 comprises the conclusions drawn from the results and recommendations for future work.

2. THEORETICAL BACKGROUND I: FUNDAMENTALS AND APPLICATIONS OF SUPERCRITICAL FLUIDS AND GAS EXPANDED LIQUIDS

2.1. SUPERCRITICAL FLUIDS

For every substance there is a temperature above which it can no longer exist as a liquid, no matter how much pressure is applied. Likewise, there is a pressure above which the substance can no longer exist as a gas no matter how high the temperature is raised. These points are called the supercritical temperature and supercritical pressure respectively and are the defining boundaries on a phase diagram for a pure substance shown in Figure 2.1. A supercritical fluid is a material which can behave as either liquid or gas, used in a state above the critical temperature and critical pressure where gases and liquids can coexist [1].

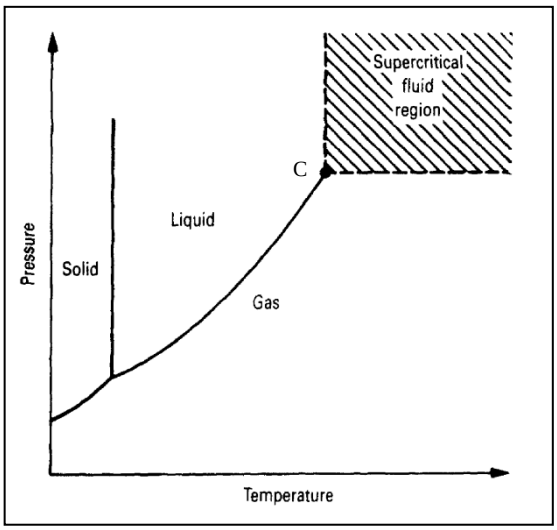

Figure 2.1. Phase diagram of a pure substance [1]

In Figure 2.1, the lines represent coexistence of the phases. If you go upward along the gas-liquid coexistence line both temperature and pressure increase. The liquid becomes less dense because of thermal expansion and the gas becomes more dense as the pressure rises. At the critical point, labeled as C in the Figure 2.1, the densities of the two phases

become identical, the distinction between gas and liquid dissapears and the line comes to an end at the critical point [1].

Table 2.1 shows critical parameters of some of the important compounds useful as supercritical fluids [3]. The applications and recent research using supercritical fluids (SCFs) as solvent or reaction media include cleaning, pharmaceuticals, food, biomaterial and polymer processing, and nanoscale processing [6]. Carbon dioxide has so far, been the most widely used because of its convenient critical temperature, cheapness, chemical stability, nonflammability, stability in radioactive applications and nontoxicity.

Table 2.1 Substances useful as supercritical fluids [3]

Substance	**Critical Temperature Tc,(K)**	**Critical Pressure Pc,(Bar)**
Carbon dioxide	304	74
Water	647	221
Ethane	305	49
Ethene	282	50
Propane	370	43
Xenon	290	58
Ammonia	406	114
Nitrus oxide	310	72
Fluoroform	299	49

Mass transfer processes become efficient due to enhanced transport properties of SCFs. SCF have diffusivities at least an order of magnitude higher, and viscosities at least an order of magnitude lower than a liquid solvent [7]. Also low surface tension of SCFs allows penetration into microporous materials which would extract liquid or gaseous medium in pores. SCFs are used for purification processes due to solvating power and selectivity.

2.1.1. Supercritical CO_2 As A Solvent Media

Carbon dioxide, in its supercritical state, is being used to replace conventional organic solvents in chemical processes.

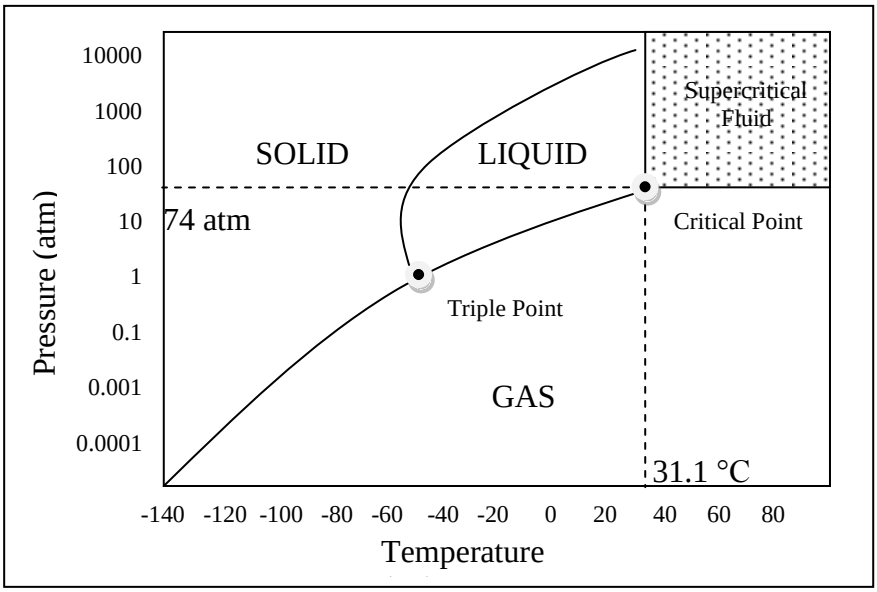

Figure 2.2. Phase behaviour of CO_2

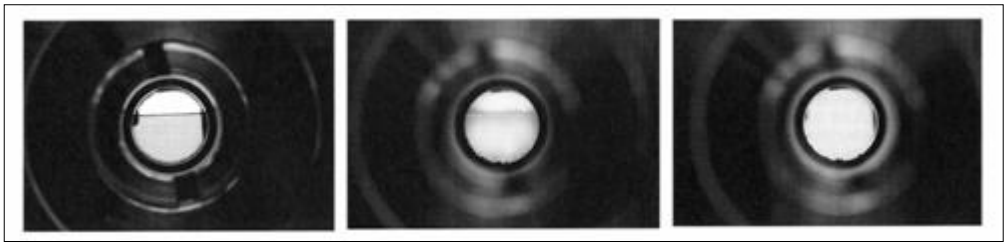

Figure 2.3. CO_2 becoming a SCF [8]

The phase behavior of CO_2 is represented in Figure 2.2. The meniscus between the liquid and gas phases disappears upon reaching the critical point, which is observed for CO_2 in a visible high pressure vessel in Figure 2.3.

A large number of industrial chemical reactions occur in organic solvents which include chlorofluorocarbons, benzene, and carbon tetrachloride-all of which have such

environmental downside such as toxicity or damage to the stratosphere ozone layer. Many of these solvents are among the ten most released chemicals to the environment. Supercritical carbon dioxide has been identified as a promising environmentally benign solvent. It is an energy conserving, selective and waste reducing alternative to organic solvents. Fast and sensitive organic synthesis can be achieved with high levels of functionality, controllability and energy efficiency [8].

The attractiveness of CO_2, as a commercial solvent is tied to its chemical and physical properties; it exists naturally as a non-flammable, virtually inert gas which is readily available and inexpensive [9].

The high compressibility of near-critical CO_2 and the dependence of solubility, transport and other properties on density allow solvent quality to be widely varied by simple pressure control without introducing a phase interface [10].

Solubility of a compound in carbon dioxide can be enhanced by cosolvents and entrainers associated with increased intermolecular interactions between solute and solvent molecules [11]. Solubility of a compound in a multi-component CO_2 mixture can be higher than the solubility of the component in pure CO_2 due to the entrainer effect [12].

2.1.2. Supercritical Drying

Supercritical drying is a process to remove liquid in a precisely controlled way, commonly used in the production of aerogels and in the preparation of biological specimens for scanning electron microscopy.

In evaporation method of drying the liquid is forced to cross the liquid-gas boundary (shown as green arrow in Figure 2.4) the substance volatilizes which causes the volume of the liquid to decrease. As this happens, surface tension at the solid-liquid interface pulls against any structures that the liquid is attached to. Delicate structures tend to be broken apart by this surface tension as the interface moves by.

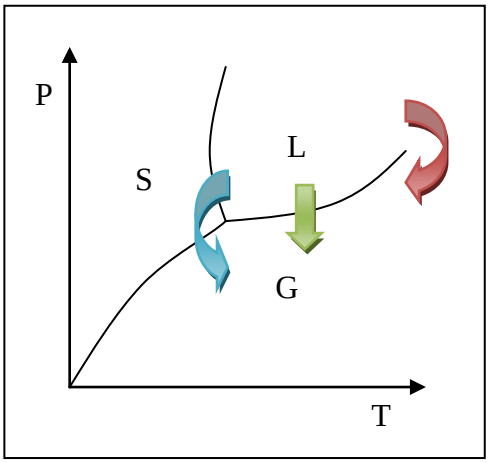

Figure 2.4. Differences between drying methods [13]

To avoid this, the sample can be brought from the liquid phase to the gas phase without crossing the liquid-gas boundary on the phase diagram; in freeze-drying, this means going around to the left (shown as blue arrow in Figure 2.4). However, some structures are disrupted even by the solid-gas boundary. Supercritical drying, on the other hand, goes around the line to the right (shown as red arrow in Figure 2.4), on the high-temperature, high-pressure side. This route from liquid to gas does not cross any phase boundary, instead passing through the supercritical region. As no boundary is crossed directly, the surface tension would not affect the structure of the sample [13].

In Figure 2.5. there are two samples of wood which had same sizes before drying. Supercritical drying and normal drying. When dried with air, drying has resulted in structural collapse and partial fragmentation of the wood. Supercritical drying replaces the liquid with a gas beyond its critical values then the supercritical fluid is removed from the medium by decompressing the fluid [14].

2.1.3. Aerogels

Supercritical drying has been very useful for the processing of highly porous aerogels. An aerogel is manufactured material with the lowest bulk density of any known porous solid.

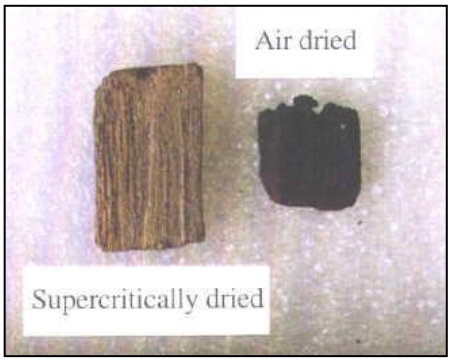

Figure 2.5. Samples dried by supercritical drying and air drying [14]

It is derived from a gel in which the liquid component of the gel has been replaced with a gas. The result is an extremely low-density solid, with a notable effectiveness as a thermal insulator (see Figure 2.6).

Essentially an aerogel is the dry, low-density, porous, solid framework of a gel (the part of a gel that gives the gel its solid-like cohesiveness) isolated in-tact from the gel's liquid component (the part that makes up most of the volume of the gel). Aerogels are open-porous (that is, the gas in the aerogel is not trapped inside solid pockets) and have pores in the range of <1 to 100 nanometers (billionths of a meter) in diameter and usually <20 nm [15].

Records held by some specially-formulated silica aerogels;

- Lowest density solid (0.0011 g cm^{-3})
- Lowest optical index of refraction (1.002)
- Lowest thermal conductivity (0.016 W m^{-1} K^{-1})
- Lowest speed of sound through a material (70 m s^{-1})
- Lowest dielectric constant from 3-40 GHz (1.008)

The starting material of an aerogel is a gel produced by sol-gel processes.

Figure 2.6. Superinsulating property of silica aerogel [15]

2.1.4. Sol Gel Process Steps

Three approaches are used to make sol-gel process: method 1, gelation of a solution of colloidal powders; method 2 hydrolysis and polycondensation of alkoxide or nitrate precursors followed by hypercritical drying of gels; method 3, hydrolysis and polycondensation of alkoxide precursors followed by aging and drying under ambient atmospheres [16].

Sols are dispersions of colloidal particles, solid particles with diameters of 1-100 nm, in a liquid. A gel is interconnected, rigid network with pores of submicrometer dimensions and polymeric chains whose average length is greater than a micrometer [17].

As an example a silica gel may be formed by network growth from an array of discrete colloidal particles (method 1) or by formation of an interconnected 3D network by the simultaneous hydrolysis and condensation of an organometallic precursor (methods 2 and 3). When the pore liquid is removed as a gas phase from the interconnected solid gel network under supercritical conditions, the network does not collapse and a low density aerogel is produced. When pore liquid is removed at or near ambient pressure by thermal evaporation and shrinkage occurs, the product is termed a xerogel as shown in Figure 2.7.

In method 1 a suspension of colloidal powders, or sol, is formed by mechanical mixing of colloidal particles in water at a pH that prevents precipitation. In methods 2 and 3 a liquid alkoxide precursor, such as Si(OR), where R is CH_3, CzH_5, or C_3H_7, is hydrolyzed by mixing with water.

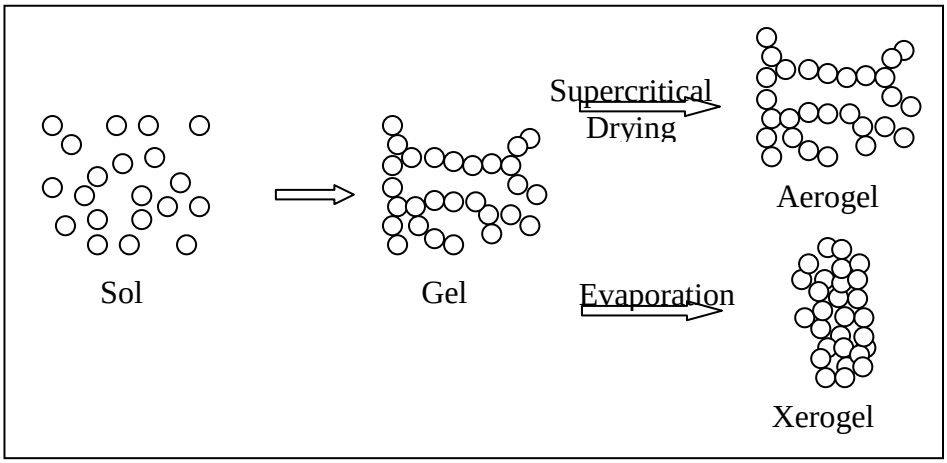

Figure 2.7. Formation of aerogel and xerogel

The hydrated silica interacts in a condensation reaction forming ≡Si-O-Si≡ bonds. Linkage of additional ≡Si-OH tetrahedra occurs as a polycondensation reaction and eventually results in SiO_2 network. The H_2O and alcohol expelled from the reaction remains in the pores of the network [16].

Hydrolysis:

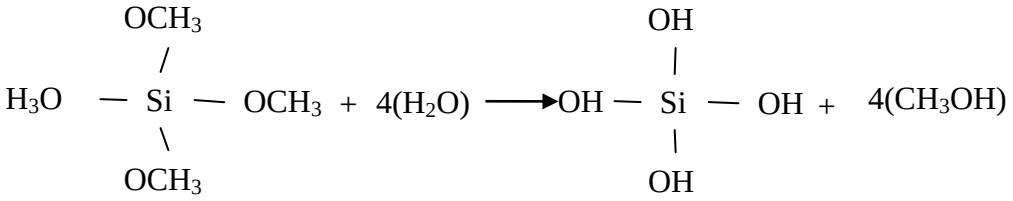

(2.1)

Condensation:

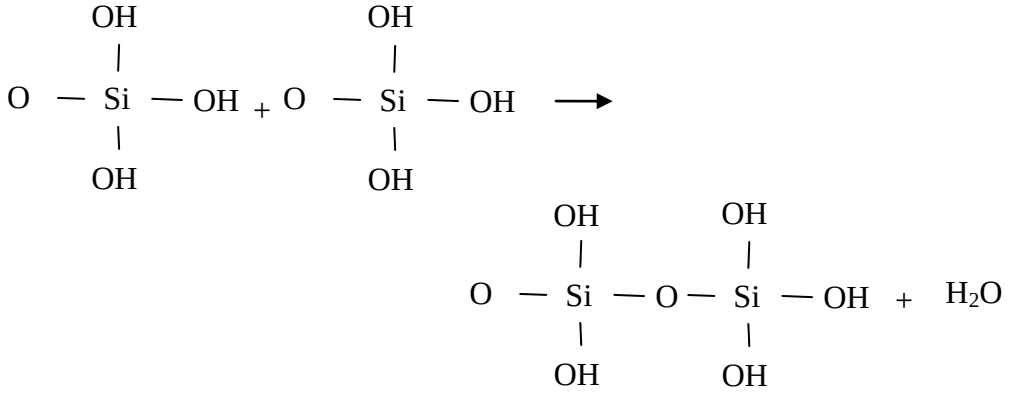

(2.2)

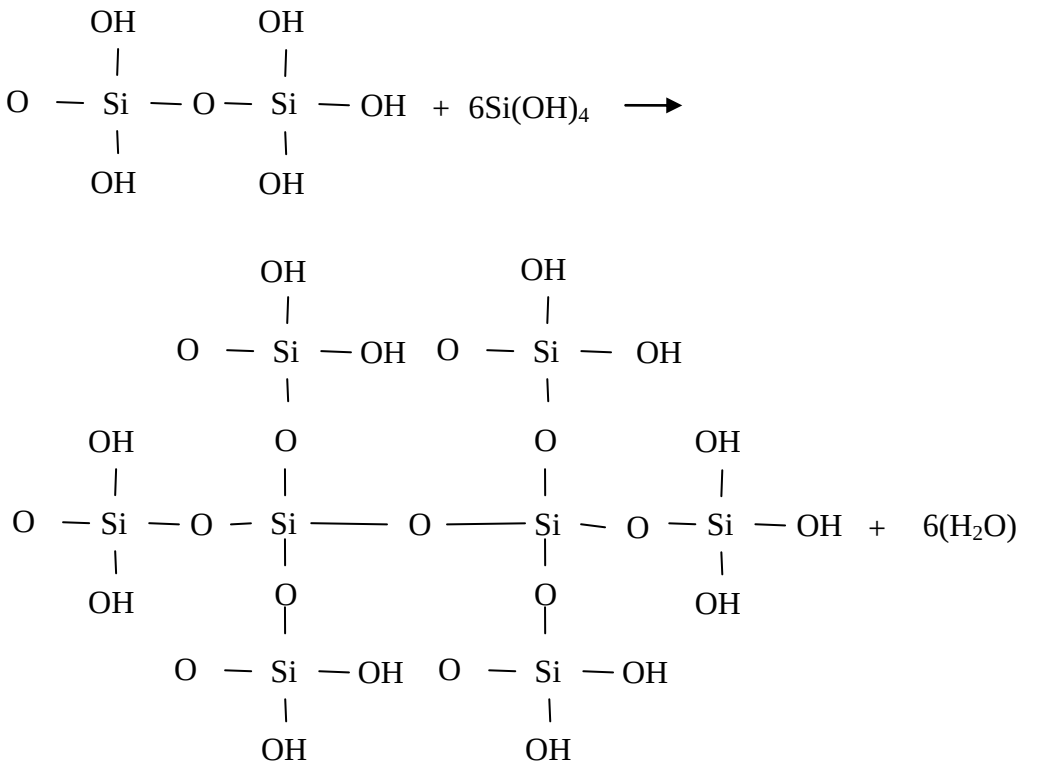

(2.3)

In a recent study, a mechanistic model for supercritical drying of a silica aerogel with supercritical carbon dioxide was developed. Here, it was proposed that, due to the dissolution of carbon dioxide in the pore liquid (ethanol), a gas-expanded liquid system formed and the pore liquid was removed more by spillage rather than convective evaporation [18].

2.2. GAS EXPANDED LIQUIDS

A gas-expanded liquid (GXL) is a mixed solvent composed of a compressible gas (such as CO_2 or ethane) dissolved in an organic solvent. CO_2-expanded liquids (CXLs) are the most commonly used class of GXLs, representing a continuum of liquid media ranging from the neat organic solvent to supercritical CO_2 [19].

Gas expanded liquids combine the beneficial properties of compressed gases such as CO_2 and of traditional solvents, leading to a new class of tunable solvents that are often the ideal type of solvents for a given application while simultaneously reducing the environmental burden. In recent years, several research groups have clearly demonstrated

how these relatively new solvents are promising alternative media for performing separations, extractions, reactions, and other applications.

2.2.1. Carbon dioxide-Expanded Liquids

Because of the safety and economic advantages of CO_2, CO_2-expanded liquids (CXLs) are the most commonly used class of GXLs.

If CO_2 is present during a reaction in a liquid solvent, then the presence of CO_2 can have a substantial effect on the reaction rate by a phenomenon called gas-expansion of the liquid phase. Dissolution of CO_2 into a liquid phase at pressures above 40 bars causes an observable and typically multi-fold increase in the volume of the liquid phase, accompanied by changes in the physical properties of the liquid phase mixture [20].

Not all liquids expand equally in the presence of CO_2 pressure, the differences are attributed to differences in the ability of the liquids to dissolve CO_2. In this regard, liquids can be divided into three general classes.

Class 1 liquids such as water have insufficient ability to dissolve CO_2 and, therefore, do not expand significantly. Also, except acidity, they have no essential change in their properties.

Class 2 liquids such as methanol, hexane and most other traditional organic solvents, dissolve large amounts CO_2, expand greatly. They consequently undergo significant changes in virtually every physical property. Volumetric expansion of class 2 solvents is dependent on the mole fraction of CO_2 in the liquid phase and independent of the choice of solvent.

Class 3 liquids such as ionic liquids, liquid polymers, and crude oil, dissolve only moderate amounts of CO_2 and, therefore, expand only moderately in volume. Some properties such as viscosity change significantly while others, such as polarity do not. The failure of class 3 solvents to expand is primarily due to their poor ability to dissolve CO_2 and not because of inability to expand in portion to the amount of CO_2 dissolved [2].

At certain temperatures and pressures, equilibrium of the CO_2 and the liquid exists, whereby both the liquid component and the CO_2 partition between two phases: some of the liquid will volatilize or solubilize into the vapor/fluid phase; and the CO_2 will dissolve into liquid phase [19]. Figure 2.8. illustrates the vapor-liquid equilibrium envelope of a typical GXL system: methanol and CO_2 at 40 °C. Figure 2.9. presents the phase behaviour of an ionic liquid ([bmim][PF_6]) and CO_2 system at 40 °C.

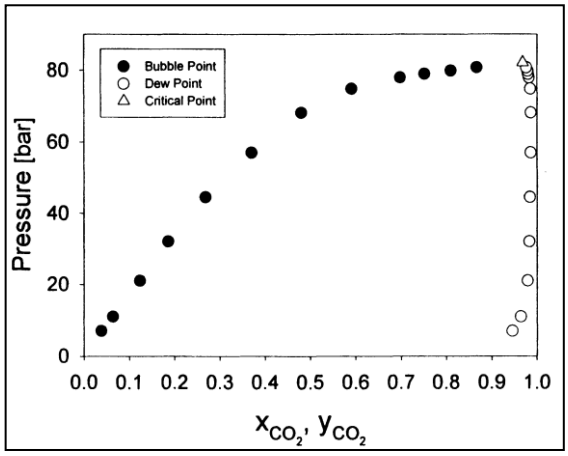

Figure 2.8. Vapor-liquid equilibrium of methanol and CO_2 at 40° C [21]

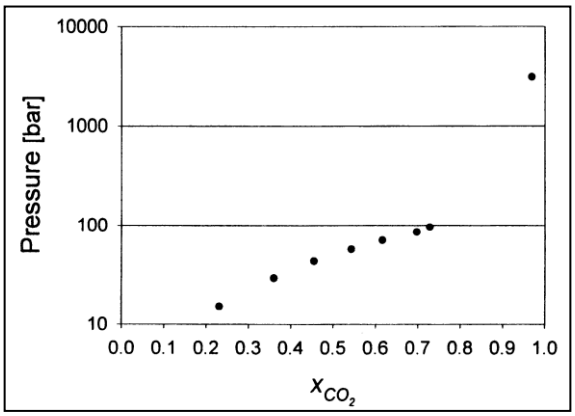

Figure 2.9. Phase behaviour of IL, [bmim][PF_6] with CO_2 at 40° C [22]

2.2.2. Applications Of Gas Expanded Liquids

In recent years, alternative media for performing chemical reactions have been the subject of many investigations. Among them, supercritical CO_2, water, CO_2-expanded

liquids (CXLs), ionic liquids (ILs) and switchable solvents have received much attention as benign media.

Supercritical CO_2 satisfies several green chemistry and engineering principles such as pollution prevention, lower toxicity and use of an plentiful resource with no increase in environmental problems.In many cases however, supercritical CO_2-based reactions are limited by inadequate solubilities of reagents or catalysts. Further, the use of CO_2 results in relatively low reaction rates for reactions that have polar transition states and requires high process pressures, typically exceeding 100 bar. These drawbacks increase reactor volumes and energy consumption, partly nullifying the environmental advantages [19].

In contrast, conventional organic solvents are chosen with dielectric properties that help solubilize the reagents and improve the rate of the desired reaction. However, the drawbacks with conventional organic solvents are toxicity and vapor emissions that may also form explosive mixtures with air.

Gas-expanded liquids (GXLs) have emerged as promising media for performing separations, extractions, reactions, and other applications. CXLs have been exploited in a variety of applications including separations, fine particle precipitation, polymer processing, and as reaction media for catalytic reactions.

By varying the CO_2 composition, a continuum of liquid media ranging from the neat organic solvent to supercritical CO_2 is generated, the properties of which can be adjusted by tuning the operating pressure; for example, a large amount of CO_2 favors mass transfer and, in many cases, gas solubility, and the presence of polar organic solvents enhances the solubility of solid and liquid solutes. CXLs have been shown to be optimal solvents in a variety of roles including inducing separations, precipitating fine particles, facilitating polymer processing, and serving as reaction media for catalytic reactions. Advantages of processing include ease of removal of the CO_2, enhanced solubility of reagent gases (compared to liquid solvents), fire suppression capability of the CO_2, and milder process pressures (tens of bars) compared to supercritical CO_2 (hundreds of bars) [2].

Applications of gas expanded liquids can be listed as below;

- GXLs are used for *media for reactions*, which yield higher reaction rates compared to other medium. As *Non catalytic reactions* in selective precipitation of a product by using CO_2 as an antisolvent can be used to overcome equilibrium limitations as shown for the synthesis of copper indomethacin in CO_2-expanded DMF [23]. During the liquid phase esterification of acetic acid with ethanol, increased conversion was observed when the reaction mixture was expanded with CO_2 (60 °C, 59 bar), possibly because of preferential partitioning of the product ester into the CO_2-rich phase, which would drive the equilibrium further to the products [24]. As *Catalytic Reactions*, the choice of the expansion gas significantly affects the rate of hydrogenation of CO_2 in liquid MeOH/NEt3 mixtures. During the asymmetric hydrogenation of 2-(6'-methoxy-2'-naphthyl)acrylic acid, an atropic acid, with [RuCl2(BINAP)(cymene)]2 in CO_2-expanded methanol, the reaction was faster but less selective than in normal methanol [25]. The properties of GXLs may also be exploited in heterogeneous catalysis. For example, adding CO_2 to an organic liquid phase in a fluid-solid catalytic system should enhance gas solubilities and improve the mass transfer properties of the expanded phase. Further, gas expanded ternary phases may be employed to reduce immiscible liquid phases to a single phase [26].
- In *polymer processing*, for a variety of polymers, CO_2 dissolution lowers the melting temperature [27], the crystallization temperature and the glass transition temperature, reduces the viscosity of the CO_2/polymer mixture, and raises the rate and degree of crystallization [28]. These effects have been exploited to manipulate particle size and morphology of polymers.
- GXLs are used in *particle formation*, for preparing fine particles several techniques [29, 30] based on CXLs have been reported in the literature for such applications as pharmaceutical compounds and explosives [31]. The processes involve either precipitation from solutions or melting of the compound followed by freezing.
- GXLs are used for *separation* and have been exploited to purify compounds and to separate mixed solutes in solution. Expansion with CO_2 was used to separate citric acid from oxalic acid and to isolate and purify p-carotene from a mixture of carotene oxidation products [32, 33].

2.3. IONIC LIQUIDS

Lately there has been an increase in research relating to the use of ionic liquids as potential replacements for organic solvents in a chemical process. Ionic liquids are generally organic salts which have a relatively low melting point when compared to inorganic salts. Many are fluid at temperatures below 298 K and these are often described as room temperature ionic liquids. However the term ionic liquid does not exclude the salts which have higher melting points which are called molten salts meaning high temperature liquids. There is no clear distinction between the term molten salt and ionic liquid [34].

Ionic liquids are made of positively and negatively charged ions. The structure of ILs is similar to table salt, sodium chloride which contains crystals made of positive sodium ions and negative chlorine ions, not molecules. The melting point of sodium chloride is 801 °C. As the molten salts exhibit high melting points, their use as solvents in applications is very limited. However, ILs are liquid generally up to 200 °C. The reason of ILs remaining liquid at room temperature is explained as the ions do not pack well. Combination of bulky and asymmetrical cations and evenly shaped anions form a liquid phase. The low melting points are due to chemical composition. The combination of larger asymmetrical organic cations and smaller inorganic counterparts lower the lattice energy and hence the melting point of the resulting ionic medium [35].

Ionic liquids have several important properties such as: wide electrochemical window, extremely low volatility, nonflammability, corrosion resistance to plastics and carbon steels, high thermal stability up to 300 °C, high ionic conductivities, and high solvating capability. Variations in cations and anions can produce a large number of ionic liquids. Properties of ionic liquids depend on the structure of ions. Typical ionic liquid cations include *N*butylpyridimium, and 1-alkyl-3-methylimidazolium or 1,3-dialkylimidazolium. Common anions are $[Cl]^-$, $[Br]^-$, $[PF_6]^-$, and $[BF_4]^-$ [36].

2.3.1. Applications of Ionic Liquids

The chemical and physical properties of ILs bring about several application areas including reaction and synthesis media.

The application areas of ILs can be expressed as;

- Ils are used for *solvent replacement*. A majority of common solvents have potential health hazards although they are extensively utilized. Therefore, environmentally friendly ILs can easily replace the hazardous solvents. ILs are able to dissolve a variety of solutes. They can be used instead of traditional solvents in liquid–liquid extractions where hydrophobic molecules such as simple benzene derivatives will partition to the IL phase [37].
- For *purification of gases*, the experimental studies show that some gases, especially CO_2 is highly soluble in ILs. The simulations performed explain that the anion of the IL is responsible for high gas solubility. CO_2 solubility is important due to the possibility of using supercritical CO_2 to extract solutes from Ils. Since ILs can dissolve certain gaseous species, they may be used in conventional gas absorption applications. Currently, researchers are interested in examining the potential of ILs for the separation of CO_2 from flue gases emitted from fossil–fuel combustion operations [38].
- ILs offer the advantages of both *homogenous and heterogeneous catalysts* with their two main characteristics: A selected IL may be immiscible with the reactants and products, but on the other hand the IL may also dissolve the catalysts. ILs combine the advantages of a solid for immobilizing the catalyst, and the advantages of a liquid for allowing the catalyst to move freely [39].
- ILs are used as *biological reactions media* such as the synthesis of pharmaceuticals due to the stability of enzymes in ILs, and in separation processes such as the extraction of amino acids [40].

2.3.2. High Pressure Phase Behaviour of Ionic Liquid-CO_2 Systems

Preliminary works have shown that supercritical CO_2 extraction is a viable method for solute recovery from an IL. However, the knowledge of phase behavior of IL–CO_2 systems is an essential aspect of this methodology. Supercritical CO_2 dissolution in the IL phase is not only necessary for contact with the solute but it also reduces the viscosity of the IL and therefore enhancing the mass transfer process [35].

2.3.2.1. The [bmim][PF_6]-CO_2 System

The studies of Blanchard et. al [22] on IL–CO_2 phase behavior indicated that these systems are very unusual biphasic systems. No measurable amount of [bmim][PF_6] was soluble in the CO_2-rich phase, although a large amount of CO_2 dissolved in the IL-rich phase, reducing the viscosity of IL. This different phase behavior is the key phenomena which makes extraction of solutes from IL with CO_2 attractive.

In their study the solubility of CO_2 in [bmim][PF_6] was determined at 40, 50 and 60 °C and pressures up to 93 bar. As the pressure increases, the solubility of CO_2 in the IL-rich phase increases dramatically and the solubility value reaches a mole fraction of 0.72 at 40 °C and 93 bar. A general rule suggests that an increase in temperature results with a decrease in the solubility of gases in liquids. As expected, the solubility of CO_2 in [bmim][PF_6] rich phase decreases with temperature. However, they noticed that the temperature dependence of the solubility is quite small in this temperature and pressure range. Another crucial point is the effect of large degree of CO_2 solubility on the viscosity of IL. The viscosity of IL decreases when a certain amount of CO_2 is dissolved in IL. This reduction in viscosity of the liquid facilitates the solution process [22].

2.3.2.1. The Other Ionic Liquids-CO_2 System

Aki et al. [41] also presented the solubility of CO_2 in ten different imidazolium-based ILs at 25, 40, and 60 °C and pressures to 150 bar. They concluded that the solubility of CO_2 in imidazolium-based ILs increases with increasing pressure and decreases with increasing temperature for all the ILs investigated.

CO_2 is the least soluble in the two ILs with non-fluorinated anions, [NO_3] and [DCA], and it has the highest solubility in ILs with anions containing fluoroalkyl groups, [TfO], [Tf_2N], and [methide].

3. THEORETICAL BACKGROUND II: DIFFUSION AND NUMERICAL TREATMENT OF THE DIFFUSIONAL PROCESS INVOLVING A MOVING INTERFACE

3.1. DIFFUSION

Diffusion is the process by which matter is transported from one part of a system to another as a result of random molecular motions.

First Fick (1855) put diffusion on a quantitative basis by adopting the mathematical equation of heat conduction derived by Fourier [42].

Diffusion processes may be divided into two types as steady state and unsteady state diffusion. Steady state diffusion takes place at a constant rate, once the process starts the number of atoms (or moles) crossing a given interface (the flux) is constant with time. This means throughout the system concentration change with respect to distance is constant and concentration change with respect to time is 0. Unsteady state diffusion is a time dependent process in which the rate of diffusion is a function of time. Thus, concentration change due to distance varies with time; and concentration change with respect to time is not 0. Both types of diffusion are described by Fick's laws of diffusion. The first law concerns both steady and unsteady state diffusion, however the second law deals only with unsteady state diffusion [43].

3.1.1 Fick's First Law Of Diffusion

Considering the flux of diffusing particles (atoms, molecules or ions) Fick's first law can be written as;

$$J=-D\frac{\partial C}{\partial z} \tag{3.1}$$

Where J is the flux of the particles and C is their concentration. The negative sign in the equation indicates opposite directions of diffusion flux and concentration gradient.

Diffusion is a process which leads to an equalisation of concentration. The factor proportionality, D, is denoted as the diffusion coefficient or as the diffusivity of the species considered [44].

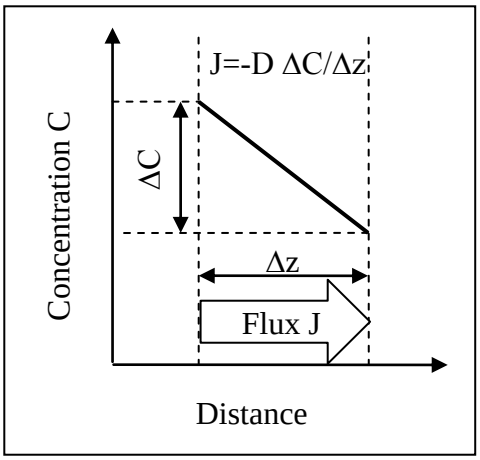

Figure 3.1. Illustration of Fick's first law [44]

3.1.2. Diffusion In Binary Mixtures

Traditionally chemical engineers have developed their design procedures for separation and reaction equipment using Fick's law of diffusion as a basis. Fick's law postulates a linear dependence of the flux J_i, with respect to the molar average mixture velocity u, and its composition gradient ∇x_i;

$$J_i=c_i(u_i-u)=-c_iD_i\nabla x_i \tag{3.2}$$

The molar flux N_i, with respect to a laboratory-fixed coordinate reference frame is given by;

$$\begin{gathered} N_i\equiv c_iu_i=c_tx_iu_i=J_i+x_iN_t=-c_tD_i\nabla x_i+x_iN_t \\ N_t=\sum_{i=1}^{n}N_i \end{gathered} \tag{3.3}$$

Ficks diffusivity is clearly necessary to adopt more general constitutive relation. The essential concepts behind such a general constitutive relation were available more than a century ago following the pioneering works of James Clerk Maxwell and Josef Stefan [45].

To affect relative motion between the molecular species of a simple two component system (species 1 and 2) a force must be exerted on each of the two species. To calculate the force exerted on any molecular species i, z-directional diffusion in the system is considered, in the control volume shown in Figure 3.2.

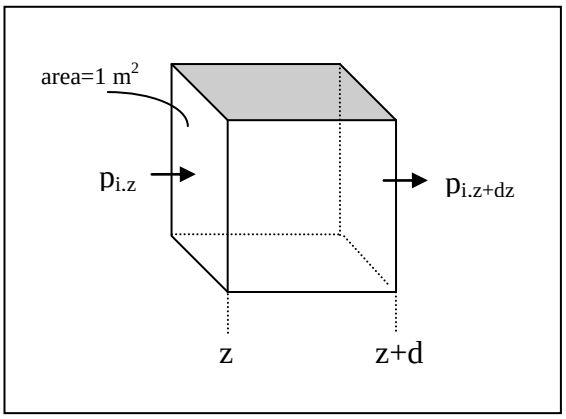

Figure 3.2. Control Volume

The cross sectional area available for diffusion is 1 m^2 and the length of the diffusion path is dz. If the change in partial pressure of component i across the diffusion path dz is $-dp_i$, the force acting per m^3 is $-dp_i/dz$. The concentration of species i in the mixture is c_i and therefore the force acting per mole of species is $(1/c_i)(-dp_i/dz)$. For an ideal gas mixture $c_i=p_i/RT$ so the relation can be written as $(RT/p_i)(-dp_i/dz)=RT(-d\ln p_i/dz)$ or expressed in terms of the chemical potential gradient, at constant temperature and pressure, of species i, this force is $-d\mu_i/dz$. This force is balanced by friction between the diffusing species 1 and 2 in the binary mixture. The force balance on the species takes the form;

$$-\frac{d\mu_1}{dz}=\frac{RT}{Đ}x_2(u_1-u_2) \tag{3.4}$$

For transport of species 1 in the positive z direction i.e. positive velocity u_1, a positive value for $(-d\mu_i/dz)$ must exist therefore the left member of equation 3.4 must be

viewed as the driving force for transport in the positive z direction. This force is balanced by the friction experienced between the species 1 and 2. The frictional drag is proportional to the velocity difference (u_1-u_2) and to the concentration of the mixture as the mole fraction of component 2, x_2. The term (RT/Đ) of the right-hand side of equation 3.4 may be interpreted to be the drag coefficient. With this definition Maxwell-Stefan diffusivity Đ has the units (m^2s^{-1}) and the physical significance of an inverse drag coefficient [3].

Multiplying both sides of the equation 3.4 by (x_1/RT), eq. Fdsı is obtained;

$$-\frac{x_1}{RT}\frac{d\mu_1}{dz}=\frac{x_1x_2u_1-x_1x_2u_2}{Đ} \tag{3.5}$$

Rearranging equation 3.5 using the definition for the fluxes $N=c_1x_1u_1$ after vector generalization is obtained;

$$-\frac{x_1}{RT}\nabla_{T,p}\mu_1=\frac{x_2N_1-x_1N_2}{c_1Đ} \tag{3.6}$$

For a non-ideal fluid mixture the component activity coefficients may be introduced to express the left member of equation 3.6 as;

$$-\frac{x_1}{RT}\nabla_{T,p}\mu_1=-\left(1+x_1\frac{\partial \ln\gamma_1}{\partial x_1}\right)\nabla x_1=-\Gamma\nabla x_1 \tag{3.7}$$

Where Γ is the thermodynamic correction factor portraying the non-ideal behaviour. Combining equations 2, 6 and 7 after introducing $x_2=(1-x_1)$;

$$J_1\equiv N_1-x_1N_t=-c_tĐ\Gamma\nabla x_1 \tag{3.8}$$

Comparison of equation 3.8 with Fick's law equation 3.2 applied to binary system of species 1 and 2 yields equation 3.9.

Equation 3.9 represents the relationship between the Fick Diffusivity D and the Maxwell-Stefan diffusivity Đ;

$$D=Đ\Gamma \tag{3.9}$$

For gaseosus mixtures at low to moderate pressures and for thermodynamically ideal liquid mixtures the thermodynamic factor Γ is equal to 1 and, furthermore, the Maxwell-Stefan diffusivity is independent of composition; for this limiting case the Fick and Maxwell-Stefan diffusivities are identical to each other.

The thermodynamic correction factor Γ defined in terms of an excess Gibbs (g^E) energy expression accounts for the nonideal behaviour of the mixture

$$\Gamma=1+x_1 \left.\frac{\partial \ln\gamma_1}{\partial x_1}\right|_{x_2,T,P} \tag{3.10}$$

At high pressures the thermodynamic correction factor is calculated with derivatives of fugacity coefficients as in the equation 3.11.

$$\Gamma=1+x_1 \left.\frac{\partial \ln\varphi_1}{\partial x_1}\right|_{x_2,T,P} \tag{3.11}$$

Hence, the problem of modelling diffusion fluxes is shifted towards the accurate determination of diffusion coefficients. With equation D=ĐΓ the diffusivities can be transformed into one another. Therefore, the Fick model and the Maxwell-Stefan equation may be employed in the description of diffusion fluxes once information on either type of diffusivity is available [46]. Maxwell-Stefan formulation also provides a way to determine the matrix of Fick diffusivities in a multicomponent mixture through the following equation [3].

$$[D] = [B]^{-1}[\Gamma] \tag{3.12}$$

Matrix B which represents the drag effects are decoupled from the thermodynamic effects represented by matrix Γ. It becomes easier to derive physical interpretations from the elements of the Fick diffusivities matrix.

3.2. NUMERICAL TREATMENT OF THE MOVING INTERFACE

A boundary value problem in one dimension is an ordinary differantial equation together with conditions involving values of the solution or its derivatives at two or more points. In a boundary value problem main aim is to satisfy a steady state solution everywhere in space that agrees with prescribed boundary conditions. When the boundary is stationary and a steady state problem exists, the problem is called a free boundary problem. And when the boundary moves with respect to time the problem is called a moving boundary problem. Free or moving boundary problems are also called Stefan problems in literature [47].

The treatment of moving interface was initially formulated and solved analytically by Stefan for simple geometry and boundary conditions. For more general conditions numerical trearment should be applied. Various numerical methods are studied in order to solve Stefan problems. Murray-Landis method is based on an equidistant movable grid finite difference method. In this method position of the interface always coincide with a grid. On the other hand Zhou and North method is based on a fixed grid finite difference method, in which the grids are fixed and a fractional parameter is used to define the distance of interface between the neighboring grids [48].

3.2.1. The Movable Grid Method

Murray and Landis kept the number of space intervals between x=0 and x=f(t), i.e. between a fixed and a moving boundary, constant and equal to I for all time. Thus, for equal space intervals $\Delta x=f(t)/I$ is different in each time step. The moving boundary is always on the i^{th} grid line [49]. Figure 3.3. illustrates the Murray-Landis movable grids.

At the beginning of each time step the interfacial fluxes and change of concentration profile due to diffusion inside each phase are calculated by assuming a stationary phase. Then, the interface moving velocity is calculated.

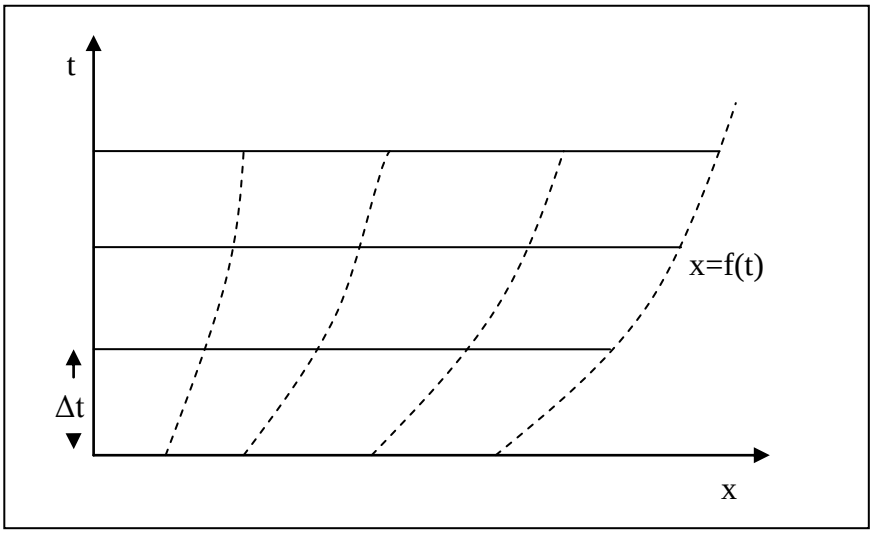

Figure 3.3. Murray and Landis Variable Grid [49]

3.2.2. The Fixed Grid Method

In fixed grid method, the interface of the two phases lies between fixed grid points as shown in Figure 3.4.

The interface lies between the m^{th} and $(m+1)^{th}$ grid. The position of the interface is denoted using a fractional parameter p ($0 \leq p \leq 1$). The parameter is defined as the ratio of the distance between the grid and the interface, over the distance between two consecutive grids.

$$p = \frac{(\text{position of interface-position of m th grid})}{\Delta x} \tag{3.13}$$

The initial position of the interface can be determined from the initial amount of phases and total number of grid points.

The diffusion equation for each phase is expressed as follows in one-dimensional form;

$$\frac{\partial C^{R,L}}{\partial t} = D^{R,L} \frac{\partial^2 C^{R,L}}{\partial x^2} \tag{3.14}$$

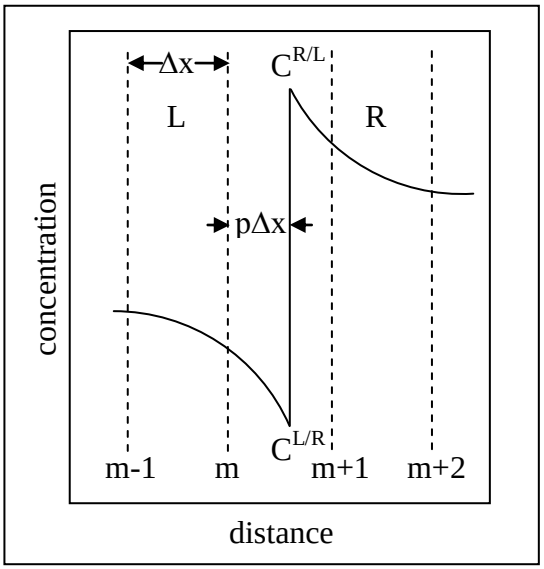

Figure 3.4. Elements of fixed grid method [50]

C^p and D^p are the concentration and the interdiffusion coefficients in phases R and L. t is time, and x represents the distance from interface. The velocity of the moving interface can be calculated by the flux balance equation.

$$\frac{d\xi}{dt}=\frac{J^{R/L}-J^{L/R}}{C^{R/L}-C^{L/R}} \tag{3.15}$$

$J^{R/L}$ and $J^{L/R}$ are the diffusional fluxes at the interface on the R and L phase side, respectively, and can be expressed as

$$J^{R/L}=-D^R\left(\frac{\partial C^R}{\partial x}\right)_{interface} \tag{3.16}$$

$$J^{L/R}=-D^L\left(\frac{\partial C^L}{\partial x}\right)_{interface} \tag{3.17}$$

The equations 3.15 and 3.16, are expressed by the ordinary finite difference method based on equidistant grids as follows:

$$\frac{\partial C_i^j}{\partial t}=\frac{C_i^{j+1}-C_i^j}{\Delta t} \tag{3.18}$$

$$D\frac{\partial^2 C_i^j}{\partial x^2}=D\frac{C_{i+1}^j-2C_i^j+C_{i-1}^j}{(\Delta x)^2} \tag{3.19}$$

$$J^{R/L}=-D^R\frac{-3C^{R/L}+4C_2^j-C_3^j}{2\Delta x} \tag{3.20}$$

$$J^{L/R}=-D^L\frac{3C^{L/R}-4C_{m-1}^j+C_{m-2}^j}{2\Delta x} \tag{3.21}$$

The superscript j means j^{th} time step and subscript i means i^{th} grid point. m is the total number of grid points in the L phase.

The distances between the interface and the neighbouring grid points are different from the intergrid distance, so special equations are required for the second derivatives of concentration at those grid points and for the concentration gradients at the interface.

Crank [51] suggested the equations below for second derivatives of concentration by using Lagrangian interpolation. However, the equations have singularities for the values p=1 and p=0.

$$\left(\frac{\partial^2 C}{\partial x^2}\right)_m=\frac{2}{(\Delta x)^2}\left[\frac{C_{m-1}}{1+p}-\frac{C_m}{p}+\frac{C^{L/R}}{p(1+p)}\right] \tag{3.22}$$

$$\left(\frac{\partial^2 C}{\partial x^2}\right)_{m+1}=\frac{2}{(\Delta x)^2}\left[\frac{C^{R/L}}{(1-p)(2-p)}-\frac{C_{m+1}}{1-p}+\frac{C_{m+2}}{2-p}\right] \tag{3.23}$$

At the interface, the concentration gradients are expressed as below;

$$\left(\frac{\partial C^L}{\partial x}\right)_{interface}=\frac{1}{\Delta x}\left[\frac{pC_{m-1}}{1+p}-\frac{(1+p)C_m}{p}+\frac{(1+2p)C^{L/R}}{p(1+p)}\right] \tag{3.24}$$

$$\left(\frac{\partial C^R}{\partial x}\right)_{interface}=\frac{1}{\Delta x}\left[\frac{(2p-3)C^{R/L}}{(1-p)(2-p)}-\frac{(2-p)C_{m+1}}{1-p}+\frac{(1-p)C_{m+2}}{2-p}\right] \tag{3.25}$$

In order to avoid the singularities at p=0 and p=1, Zhou and North [50] ignored the grid on the left of the interface, m^{th} grid in Figure 3.4, when p<0.5 and ignored the grid on the right of the interface, the $(m+1)^{th}$ grid in Figure 3.4, when p>0.5. Therefore when p<0.5 the following expressions were used for the second derivative of concentration at the $(m-1)^{th}$ grid and for the concentration gradient at interface in the left hand side phase

$$\left(\frac{\partial^2 C}{\partial x^2}\right)_{m-1} = \frac{2}{(\Delta x)^2}\left[\frac{C_{m-2}}{2+p} - \frac{C_{m-1}}{1+p} + \frac{C^{L/R}}{(1+p)(2+p)}\right] \tag{3.26}$$

$$\left(\frac{\partial C^{L}}{\partial x}\right)_{interface} = \frac{1}{\Delta x}\left[\frac{(1+p)C_{m-2}}{2+p} - \frac{(2+p)C_{m-1}}{1+p} + \frac{(3+2p)C^{L/R}}{(1+p)(2+p)}\right] \tag{3.27}$$

and when p>0.5 the following expressions were used for the second derivative of concentration at the $(m+2)^{th}$ grid and for the concentration gradient at interface in the right hand side phase.

$$\left(\frac{\partial^2 C}{\partial x^2}\right)_{m+2} = \frac{2}{(\Delta x)^2}\left[\frac{C^{R/L}}{(2-p)(3-p)} - \frac{C_{m+2}}{2-p} + \frac{C_{m+3}}{3-p}\right] \tag{3.28}$$

$$\left(\frac{\partial C^{R}}{\partial x}\right)_{interface} = \frac{1}{\Delta x}\left[\frac{(2p-5)C^{R/L}}{(2-p)(3-p)} - \frac{(3-p)C_{m+2}}{2-p} + \frac{(2-p)C_{m+3}}{3-p}\right] \tag{3.29}$$

Fixed grid method is more promising as it does not include the procedure for correction of concentration values on each grid point due to the displacement of the interface in movable grid method.

The value 0.5 can be named as p^* value that can be used as limitation for the above equations. By decreasing the value that is given to p^* the global mass change due to the ignorance of the grid and thus correction term can be considerably reduced. However smaller values of p^* allows the interface to be located close to the neighbouring grid points, and this causes a decrease of the time increment which yields increase in computing time [52].

The amount of global mass change due to the displacement of interface by $\Delta\xi$ can be obtained by calculating the difference of mass between m th and $(m+1)^{th}$ grid. The following equation is obtained;

$$\Delta m=\Delta\xi\,(C^{R/L}+C_{m+1}-C^{L/R}-C_m)/2 \tag{3.30}$$

Then a new flux balance equation can be derived and with equation 3.30 the amount of interface displacement $\Delta\xi$ can be calculated.

$$\frac{\Delta\xi}{\Delta t}=\frac{2(J^{R/L}-J^{L/R})}{(C^{R/L}+C_{m+1}-C^{L/R}-C_m)} \tag{3.31}$$

4. THEORETICAL BACKGROUND III: THERMODYNAMIC MODELING OF PHASE EQUILIBRIUM

4.1. BASIC THERMODYNAMICS OF PHASE EQUILIBRIUM

The thermodynamic requirement for a phase equilibirium is that the temperature, pressure and partial molar Gibbs free energy of each species must be same in all phases.

In the equation below, the superscript I defines the phase in which species i, denoted as a subscript, is present.

$$\overline{G_i}^{I}(x_i^{I},T,P)=\overline{G_i}^{II}(x_i^{II},T,P)=\overline{G_i}^{III}(x_i^{III},T,P)=\ldots \tag{4.1}$$

$$\overline{G_i}^{I}(x_i^{I},T,P)=\left[\frac{\partial(N^{I}\underline{G}^{I})}{\partial N_i^{I}}\right]_{N^{I}_{k\neq i},T,P}=\mu_i^{I}(x_i^{I},T,P) \tag{4.2}$$

Here T and P are temperature and pressure respectively, x_i represents all the mole fractions in the phase I, $\underline{G}^{I}$ is the molar Gibbs free energy of the phase and the subscript $N^{I}_{k\neq i}$ indicates that the derivative is to be taken with respect to the number of moles of species i in the phase I with all other mole numbers held constant. The partial molar Gibbs free energy of a species is equal to its chemical potential μ_i [3].

With equations of state, real mixture behaviour is described by introducing fugacity, f. The fugacity of a species in a real mixture is;

$$\overline{f_i}(T,P,x_i)=x_i f_i(T,P)\exp\left[\frac{\overline{G_i}(T,P,x_i)-\overline{G_i}^{IM}(T,P,x_i)}{RT}\right] \tag{4.3}$$

where $f_i(T,P)$ is the pure component fugacity of the species at the temperature and pressure of the mixture. A fugacity coefficient is defined as;

$$\overline{\varphi_i}(T,P,x_i)=\frac{\overline{f_i}(T,P,x_i)}{x_iP} \tag{4.4}$$

For a system to reach thermodynamic equilibrium the fugacity of each species must be the same in all phases.

$$\overline{f_i}^{L}(x_i,T,P)=\overline{f_i}^{V}(y_i,T,P) \tag{4.5}$$

where superscripts L and V represent liquid and vapor, respectively and y_i is the mole fraction of species i in the vapor. For the vapor phase equations of state are used to calculate fugacities. However, the activity coefficient models can also be used for the liquid phase.

When an equation of state is used to describe the fugacity in the vapor phase, the equation to be used would be;

$$\ln\left[\frac{\overline{f_i}^{V}(y_i,T,P)}{y_iP}\right]=\ln\overline{\varphi_i} \tag{4.6}$$

$$=\frac{1}{RT}\int_{V=\infty}^{V}\left[\frac{RT}{V}-\left(\frac{\partial P}{\partial N_i}\right)_{T,V,N_{j\neq i}}\right]dV-\ln Z^V \tag{4.7}$$

In the equation 4.7 V is the total volume, and Z is the compressibility factor computed from an equation of state [3].

Among the activity coefficients used for liquid phase calculations Non-Random Two Liquid (NRTL) model is the most notable one. It has the advantage of having three adjustable parameters that allow it to be used for fitting the phase behaviour of highly nonideal mixtures. For a binary mixture NRTL model equations are;

$$\ln\gamma_1=x_2^2\left[\tau_{21}\left(\frac{G_{21}}{x_1+x_2G_{21}}\right)^2+\frac{\tau_{12}G_{12}}{(x_2+x_1G_{12})^2}\right] \tag{4.8}$$

$$\ln\gamma_2 = x_1^2\left[\tau_{12}\left(\frac{G_{12}}{x_2+x_1G_{12}}\right)^2+\frac{\tau_{21}G_{21}}{(x_1+x_2G_{21})^2}\right] \quad (4.9)$$

with

$$\ln G_{12} = -\alpha_{12}\tau_{12} \quad (4.10)$$

$$\ln G_{21} = -\alpha_{21}\tau_{21} \quad (4.11)$$

where α_{12} and α_{21} are called non-randomness parameter, for which usually α_{12} is set equally α_{21}. For liquid-liquid equilibria α values are usually set to 0.2 and for vapor- liquid equilibria values are set to 0.3 [53].

4.2. EQUATIONS OF STATE

An equation of state is a formula describing the interconnection between various macroscopically measurable properties of a system. For physical states of matter, this equation usually relates the thermodynamic variables of pressure, temperature, volume and number of atoms to one another.

Several equations of state are described below;

- *The ideal gas law* describes gas-phase systems reasonably well at low pressure. The ideal gas model assumes that there is no interaction between gas species and it neglects the volume occupied by the gas species.
- *The van der Waals equation* of state provides a better description of gases at higher pressures than does the ideal gas law. It introduces two empirical parameters to correct for the interaction between gas atoms or molecules and for the volume occupied by the gas molecules.
- Another two parameter real gas equation is the *Redlich-Kwong equation*. It is almost always more accurate than the van der Waals equation and often more accurate than some equations with more than two parameters.

- *The Peng-Robinson equation* exhibits performance similar to the Redlich-Kwong equation, although it is generally superior in predicting the liquid densities of many materials, especially nonpolar ones.

In our study, equation of state approach is used for both liquid and vapor phases Fugacity coefficients of species i in both homogeneous liquid and vapor phases are equal to:

$$\ln \overline{\varphi_i} = \ln \frac{\overline{f_i}(T,P,z_i)}{z_i P} \tag{4.12}$$

$$\ln \overline{\varphi_i} = \frac{1}{RT} \int_{v=\infty}^{v} \left[\frac{RT}{V} - \left(\frac{\partial P}{\partial N_i} \right)_{T,V,N_{j \neq i}} \right] dV - \ln Z \tag{4.7}$$

where z_i is used as a generic mole fraction term; when the equation is applied to the liquid phase x_i is substituted; for the vapor phase y_i is used instead. In the equation of state approach an equation like Peng-Robinson equation is used to obtain molar volume V_m or, equivalently, compressibility factor Z.

A single equation of state (EOS), such as the Peng-Robinson EOS, can accurately describe both the liquid and vapor phase. The Peng-Robinson EOS is part of a family of equations of state called cubic because the compressibility factor, Z, is a solution of a cubic equation [3].

$$p = \frac{RT}{V_m - b} - \frac{a(T)}{V_m(V_m + b) + b(V_m - b)} \tag{4.13}$$

The parameter ‘a’ is a function of temperature, which is for intermolecular interactions between the species in the mixture, and ‘b’ is the excluded volume parameter which is for size differences between the species in the mixture.

First to ensure that the equation of state predicts the correct critical temperature T_c and the critical pressure P_c of the mixture the following conditions were invoked at the critical point:

$$\left(\frac{\partial P}{\partial V}\right)_{T_c} = \left(\frac{\partial^2 P}{\partial V^2}\right)_{T_c} = 0 \tag{4.14}$$

This leads to

$$a(T) = 0.457235 \left(\frac{R^2 T_c^2}{P_c}\right) \alpha(T) \tag{4.15}$$

$$b = 0.77796 \left(\frac{R T_c}{P_c}\right) \tag{4.16}$$

These relations ensure that a critical point is obtained from the EOS. The term α(T) is temperature dependent and makes sure that the vapor pressure calculated from the equation of state is accurate at temperatures other than the critical temperature. This term is equal to unity at critical temperature.

$$\alpha(T) = \left[1 + \kappa\left(1 - \sqrt{T/T_c}\right)\right]^2 \tag{4.17}$$

which is applicable to hydrocarbons and organic gases with the following form for κ:

$$\kappa = 0.37464 + 1.54226\omega - 0.26992\omega^2 \tag{4.18}$$

where ω is the acentric factor defined as

$$\omega = -1.0 - \log_{10}\left[\frac{P^{vap}(T_r = 0.7)}{P_c}\right] \tag{4.19}$$

where $T_r = T / T_c$ is the reduced temperature.

The equation is completely predictive once three constants; critical temperature, critical pressure and the acentric factor are given.

Several investigators have introduced ways of adding further species-specific constants to provide accurate vapor pressure correlations, especially at lower temperatures

and for nonhydrocarbon fluids, that are needed for a better description of vapor-liquid equilibrium. The temperature dependence term α(T) modified by Stryjek and Vera is used [4]. In their approach equation 4.18 is replaced by the relation

$$\kappa=\kappa_0+\kappa_1\left(1+T_r^{0.5}\right)(0.7-T_r) \tag{4.20}$$

with

$$\kappa_0=0.378893+1.4897153\omega-0.17131848\omega^2+0.0196554\omega^3 \tag{4.21}$$

And where constant κ_1 is specific for each pure compound and is used to fit low-temperature saturation pressures accurately [3]. It is determined by fitting pure component saturation pressure to temperature.

Some of the CO_2–solute systems modeled by Peng-Robinson equation of state and its modifications include the mixtures of CO_2 with alkanes, alkenes, alcohols, ketones and esters.

4.3. MIXING-COMBINING RULES

The greatest utility of cubic equations of state is for mixture phase equilibrium calculations. The assumption is inherent in most such computations is the one-fluid model, that is that the same equation of state used for pure fluids can be used for mixtures if a way of obtaining parameters for mixtures is available [54].

Several mixing rules are mentioned below;

- In *one parameter van der waals one fluid model* It is assumed that if the two components of the mixture separately obey this principle, then their mixture may be expected to behave as if it were a single-component fluid, called the equivalent fluid, characterized by some suitable (composition dependent) average-potential parameters [5].

- In the case of *two parameter van der waals one fluid model*, the equations used for previous model are used with the exception that the binary parameter employed is now a composition dependent two parameter term [5].
- *Wong-Sandler mixing rule* produces the desired equation of state behavior at both low and high densities without being density dependent and allows extrapolation over wide ranges of temperature and pressure [54].
- The basic assumption of the *Huron-Vidal mixing rule* is the use of the infinite pressure as the reference pressure. The combinatorial and excess volume terms of the cubic EOS dissappear at infinite pressure which simplifies the mathematics [55].

In the study with the Wong-Sandler mixing rule the EOS parameters for homogeneous liquid or vapor mixture is computed as below;

$$b=\frac{RT\sum_i\sum_j z_i z_j\left(b-\frac{a}{RT}\right)_{ij}}{RT-\left[\sum_i z_i\frac{a_i}{b_i}+\frac{\underline{G}_\gamma^{ex}(T,z_i)}{C^*}\right]} \tag{4.22}$$

with

$$\left(b-\frac{a}{RT}\right)_{ij}=\frac{1}{2}\left[\left(b_i-\frac{a_i}{RT}\right)+\left(b_j-\frac{a_j}{RT}\right)\right](1-k_{ij}) \tag{4.23}$$

$$a=bRT\left[\frac{\underline{G}_\gamma^{ex}(T,z_i)}{C^*RT}+\sum_i z_i\frac{a_i}{b_iRT}\right] \tag{4.24}$$

In the equations $\underline{G}_\gamma^{ex}$ the molar excess Gibbs free-energy obtained from any excess free energy model, is a function of temperature and composition only. Eventhough the Wong-Sandler derivation involves the Helmholtz free-energy of the mixture, this substitution is due to the assumption that $\underline{G}_\gamma^{ex}(T,z_i)=\underline{A}_{EOS}^{ex}(T,P,z_i)$. The C^* term is the EOS-dependent constant. For the Peng-Robinson EOS $C^*=\left[\ln(\sqrt{2}-1)\right]/\sqrt{2}=-0.62323$.

The fugacity coefficient expressions for species i in a mixture for the Wong-Sandler mixing rule can be written as,

$$\ln \overline{\varphi}_i(T,P,z_i)=\frac{\left(\frac{\partial Nb}{\partial N_i}\right)_{T,N_{j\neq i}}}{b}(Z-1)$$

$$-\ln(Z-B)+\frac{a}{2\sqrt{2}bRT}\left\{\frac{\left[\frac{1}{N}\left(\frac{\partial N^2a}{\partial N_i}\right)_{T,N_{j\neq i}}\right]}{a}-\frac{\left[\left(\frac{\partial Nb}{\partial N_i}\right)_{T,N_{j\neq i}}\right]}{b}\right\}\times\ln\left[\frac{Z+\left(1-\sqrt{2}\right)I}{Z+\left(1+\sqrt{2}\right)}\right. \tag{4.25}$$

The partial derivative terms are

$$\left(\frac{\partial Nb}{\partial N_i}\right)_{T,N_{j\neq i}}=\frac{1}{1-D}\left(\frac{1}{N}\frac{\partial N^2Q}{\partial N_i}\right)-\frac{Q}{(1-D)^2}\left(1-\frac{\partial ND}{\partial N_i}\right) \tag{4.26}$$

$$\frac{1}{N}\left(\frac{\partial N^2a}{\partial N_i}\right)=RTD\left(\frac{\partial Nb}{\partial N_i}\right)+RTb\left(\frac{\partial ND}{\partial N_i}\right) \tag{4.27}$$

with

$$Q=\sum_i\sum_j z_iz_j\left(b-\frac{a}{RT}\right)_{ij} \tag{4.28}$$

$$D=\frac{\underline{G}_\gamma^{ex}(T,z_i)}{C^*RT}+\sum_i z_i\frac{a_i}{b_iRT} \tag{4.29}$$

$$\left(\frac{1}{N}\frac{\partial N^2Q}{\partial N_i}\right)=2\sum_j z_j\left(b-\frac{a}{RT}\right)_{ij} \tag{4.30}$$

$$\frac{\partial ND}{\partial N_i}=\frac{a_i}{b_iRT}+\frac{\ln\gamma_i}{C^*} \tag{4.31}$$

$$\ln\gamma_i=\frac{1}{RT}\left[\frac{\partial N\underline{G}_\gamma^{ex}(T,z_i)}{\partial N_i}\right]_{T,N_{j\neq i}} \tag{4.32}$$

The advantage of Wong Sandler mixing rule is that it can predict the vapor-liquid equilibria of highly nonideal mixtures containing condensable components using activity coefficient model parameters obtained at or near room temperature [3].

5. DEVELOPMENT OF THE MODEL

The model is based on the Fickian formulation of the diffusion taking place in an open system which has an ionic liquid at the bottom and dense carbon dioxide above it (see Figure 5.1).

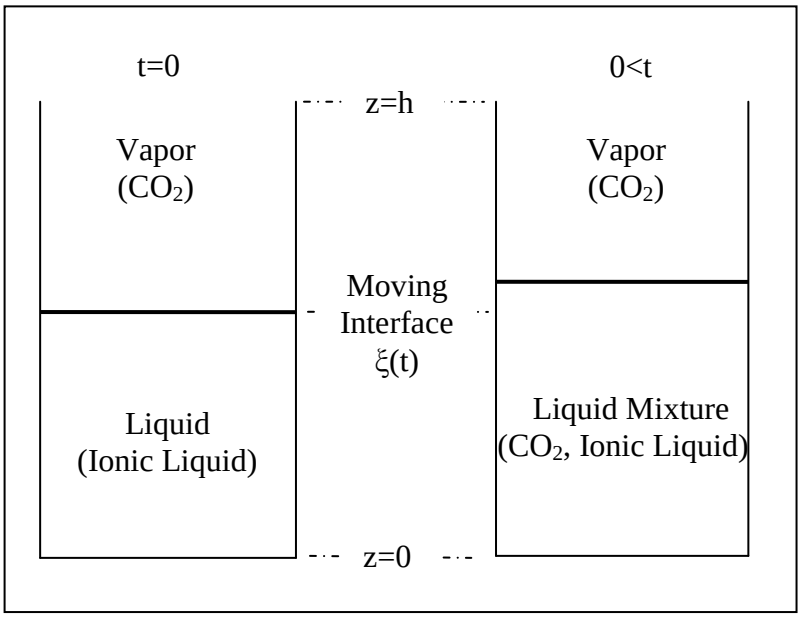

Figure 5.1. The prototype system I

The second open system has liquid methanol at the bottom and dense carbon dioxide above it (see Figure 5.2).

The unsteady state diffusion equation in one-dimensional form in terms of mole fractions is expressed as follows:

$$\frac{\partial x}{\partial t} = [D]\frac{\partial^2 x}{\partial z^2} \tag{5.1}$$

The system has two components in each case namely; carbon dioxide and methanol, carbon dioxide and ionic liquid.

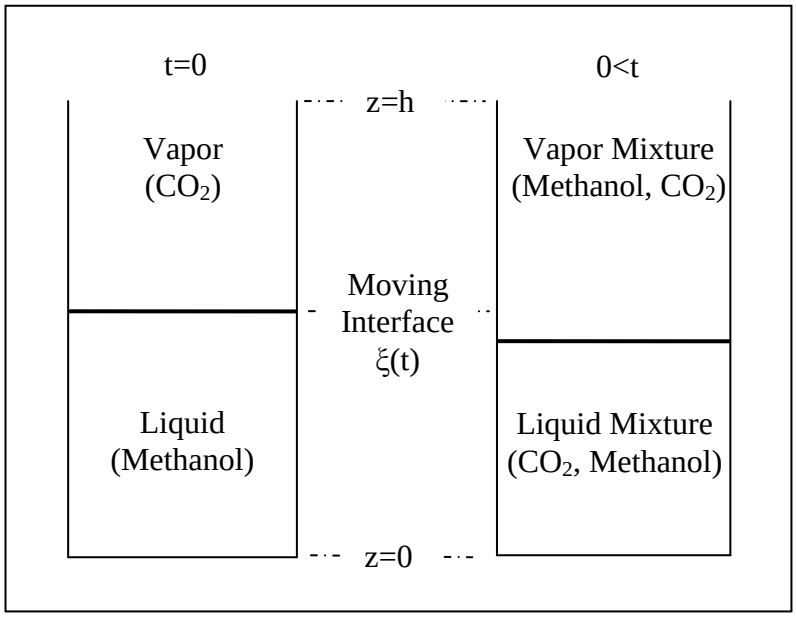

Figure 5.2. The prototype system II

Two partial differential equations will be solved simultaneously since only (n-1) equations per phase are independent, n being the number of species. The molar volumes of the phases are different from each other. This means that the volume covered by the moving interface during one time step will be different in each phase; the total volume may be not be conserved. Therefore, the space variable z is transferred into z' with a dimension of moles over area by dividing z with molar volumes. This approach ensures that the distance covered by the interface in each phase is the same in z' space even though the molar volumes are not the same [56, 57]. The transport equations in liquid and vapor phases respectively after the transformation of the axis variable are:

$$J=-\frac{1}{V_m^2}D(\nabla x) \tag{5.2}$$

$$\frac{\partial x_{CO_2}}{\partial t}=\frac{1}{V_L^2}D\frac{\partial^2 x_{CO_2}}{\partial z'^2} \tag{5.3}$$

If the liquid evaporates then the following partial derivative is solved in the vapour phase.

$$\frac{\partial y_{CO_2}}{\partial t} = \frac{1}{V_V^2} D \frac{\partial^2 y_{CO_2}}{\partial z'^2} \tag{5.4}$$

V_V and V_L for the molar volumes of the vapor and the liquid phases respectively.

The initial and boundary conditions of the system are;

- Initially, there is no carbon dioxide in the liquid and there is no ionic liquid or methanol in the dense gas.

$$x_{CO_2} = 0$$

$$y_{liquid} = 0$$

- At the top of the capillary mole fraction of CO_2 is one.

$$y|_{z=L} = 1.0$$

- At the bottom of the capillary there is no flux boundary condition, which means the mole fraction of the liquid does not change with z at z=0.

$$\left.\frac{\partial x}{\partial z}\right|_{z=0} = 0$$

- At the interface the local equilibrium condition is accepted.

$$y = Kx$$

Lee and Oh [52] have described the numerical treatment of the moving boundary using a fixed grid finite difference method. Here, the position of the interface does not necessarily coincide with a grid point. The interface lies between the (m) and $(m+1)^{th}$ grids and the exact location is indicated with a fractional parameter p, which can take any value between 0 and 1. Since the distances between the interface and the neighboring grids are not the same as the intergrid distance, special finite difference expressions are developed for them using the parameter p. The new expressions have singularities at p=0 and p=1.

Therefore, they are further modified to be used when the value of p approaches either 0 or 1 (see Section 3.2.2)

In the z space, the moving interface has different velocities in each phase as mentioned before. Here, the moving velocity of the phase interface is calculated using the flux balance equation.

$$J^{V/L}-J^{L/V}=v^{V}\frac{x^{V/L}}{V^{V}}-v^{L}\frac{x^{L/V}}{V^{L}} \tag{5.5}$$

The velocities of the phases v^{V} and v^{L} are not independent from each other and they relate each other as;

$$\frac{v^{V}}{V^{V}}=\frac{v^{L}}{V^{L}} \tag{5.6}$$

And the velocity of the interface is expressed as;

$$v^{z^{1}}\equiv\frac{\Delta\xi}{\Delta t}=\frac{2(J^{V/L}-J^{L/V})}{y^{V/L}+y_{m+1}-x^{L/V}-x_{m}} \tag{5.7}$$

In the model firstly the mole fractions at the grids away from the interface were calculated, at each iteration. Then the fractions at the neighboring grids of interface were calculated with the equations described in Section 3.2.2. Also mole fractions at the interface was calculated. Finally using the mole fractions the displacement of the interface was found.

The PRSV equation of state parameters and WS mixing rules for supercritical CO_2-methanol were optimized by using experimental data reported by Chang and Day [58] (See Appendix C)

To calculate infinite dilution diffusivity in the supercritical CO_2, the correlation proposed by He and Yu is used [59];

$$D^0_{MeOH}=\alpha*10^{-5}\left(\frac{T}{M_A}\right)^{1/2}\exp\left(\frac{0.3887}{\frac{V_B}{V_{cB}}-0.23}\right) \quad (5.8)$$

$$\alpha=14.882+0.005908\left(\frac{T_{cB}V_{cB}}{M_B}\right)+2.0821*10^{-6}\left(\frac{T_{cB}V_{cB}}{M_B}\right)^2 \quad (5.9)$$

The infinite dilution diffusivity of CO_2 in methanol is calculated at 313.15 K and 73.9 bar with the following equation;

$$D^0_{CO_2}=2.22*10^{-7}\exp\left(-\frac{9340}{RT}\right) \quad (5.10)$$

Pressure corrections on the liquid phase infinite dilution diffusivities using viscosity data for high pressures. Since diffusivity is inversely related to viscosity, the following equation is employed. Viscosity data used are tabulated in Appendix B.

$$D^0_{AB}\eta_B=\text{constant} \quad (5.11)$$

The diffusivities at different compositions are determined using the Vignes formula.

$$D_{CO_2}=D^{0\,x_m}_{CO_2}D^{0\,x_c}_{MeOH} \quad (5.12)$$

$$D_{MeOH}=D^{0\,y_m}_{CO_2}D^{0\,y_c}_{MeOH} \quad (5.13)$$

The following calculations are carried out for a capillary tube with a length of 200 mm and a diameter of 2 mm. Initially, one tenth of the capillary is filled with liquid. The temperature is 313.14 K and the pressure is 75 bars for ionic liquids and 73.9 bars for methanol. The infinite dilution diffusivities are presented in Table 5.1.

For methanol-CO_2 system the composition dependent diffusivities (Maxwell-Stefan Diffusivities) and thermodynamically corrected diffusivities (Fick Diffusivities) are calculated. The results are presented in Table 5.2.

Table 5.1. Infinite Dilution Diffusivities

$\mathbf{D_{CO_2\text{-}[bmim][PF6]}}$ **[cm²/s]**	$\mathbf{D_{CO_2\text{-}[thtdp][Cl]}}$ **[cm²/s]**	$\mathbf{D_{CO_2\text{-}MeOH}}$ **[cm²/s]**	$\mathbf{D_{MeOH\text{-}CO_2}}$ **[cm²/s]**
0.35×10^{-5}	0.30×10^{-5}	5.89×10^{-5}	4.97×10^{-4}

Table 5.2. Maxwell-Stefan and Fick Diffusivities for Methanol-CO_2 system at 73.9 bar and 313.14 K

$\mathbf{Đ_{CO_2\text{-}MeOH}}$ **[cm²/s]**	$\mathbf{Đ_{MeOH\text{-}CO_2}}$ **[cm²/s]**	$\mathbf{D_{CO_2\text{-}MeOH}}$ **[cm²/s]**	$\mathbf{D_{MeOH\text{-}CO_2}}$ **[cm²/s]**
1.33×10^{-4}	4.90×10^{-4}	1.44×10^{-4}	4.11×10^{-4}

6. RESULTS AND DISCUSSION

The expansion of methanol and two different ionic liquids, [bmim][PF_6] and [thtdp][Cl] with carbon dioxide are examined. The differential equations governing the diffusion of species in each phase and the movement of the phase interface are solved using a numerical technique based on a finite difference formulation. First, the convergence of the method is tested by using different time intervals and grid sizes. Then, the accuracy of the model is established by comparing the numerical results with the experimental data obtained by Slattery and Mhetar for the methanol-air system at ambient pressure [60].

The calculations for the aforementioned three systems are carried out using pressure-corrected infinite dilution diffusivities. The velocity of the phase interface and the average mole fraction of carbon dioxide in the liquid during the first 2500 seconds of diffusion process are presented. The composition profiles in the liquid and vapor phases are also examined. In the case of methanol, the effect of using composition-dependent Fick diffusivity on the interface velocity is also investigated.

6.1. CONVERGENCE OF THE NUMERICAL METHOD

The convergence analysis is carried out for the methanol-carbon dioxide system at high pressure (P=73.9 bar, T=313 K). Figure 6.1 shows the change in the position of the phase interface during the diffusion of carbon dioxide into methanol with time obtained using different time steps. We observe that the selected time steps produced stable solutions which overlapped during the entire time period. A time step of 0.012 is used in the rest of the calculations.

Figure 6.2. indicates the change in the position of the interface in the same system obtained using different grid sizes. In all cases, the interface displacements are found to be almost identical; the numerical solution is independent of the grid sizes. For the rest of the calculations, the number of grids is set to 480.

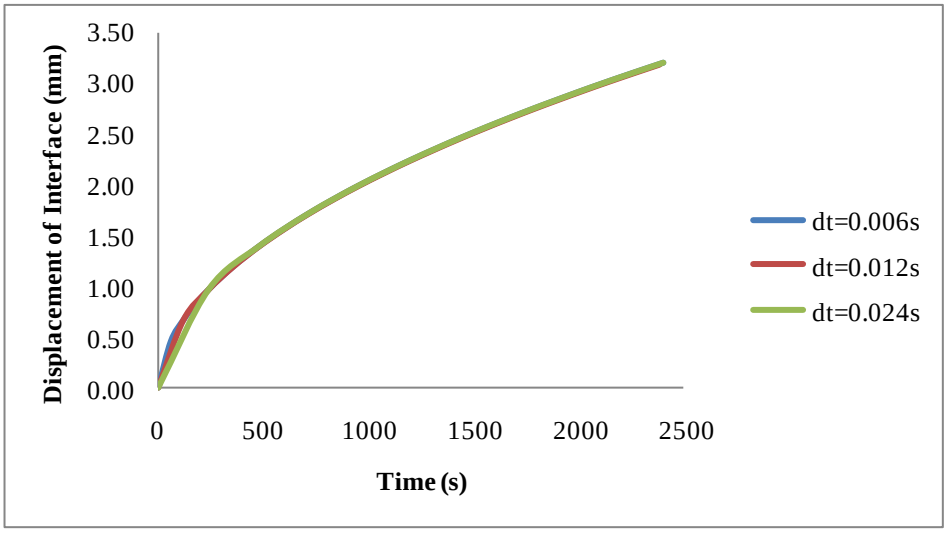

Figure 6.1. Numerical results at different time steps for methanol-CO_2 system at 73.9 bar, 313.14 K.

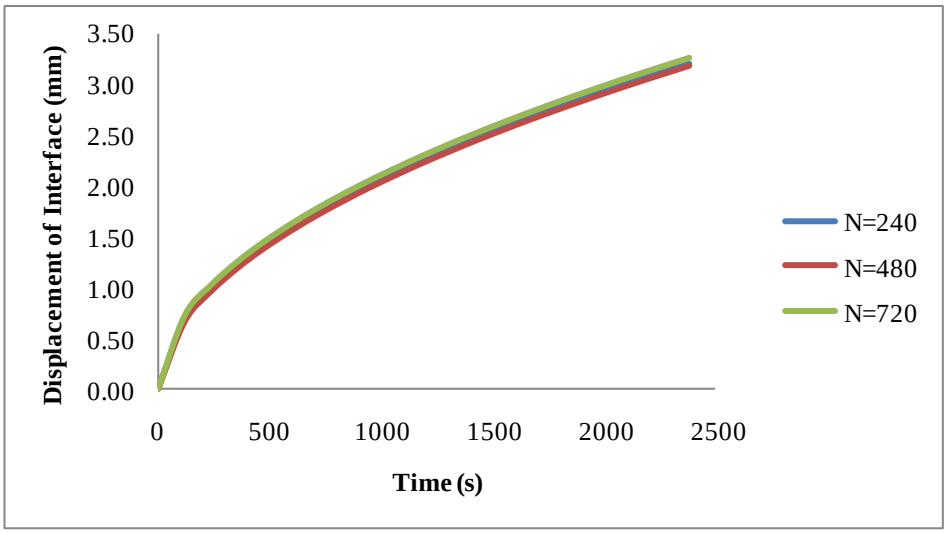

Figure 6.2. Numerical results at different grid sizes for methanol-CO_2 system at 73.9 bar, 313.14 K.

6.2. COMPARISON WITH LITERATURE DATA

The numerical procedure is tested with the binary experimental data reported by Slattery and Mhetar [60] for the evaporation of methanol into air at ambient pressure.

In this case, the pressure is low and therefore, the gas is not soluble in liquid. Mass transfer takes place only from liquid to vapor. Figure 6.3 shows the change in the position of the interface with time up to 2500 seconds. Due to the vaporization process, the interface goes down in the tube. We observe that the numerical solution compare well with the experimental data.

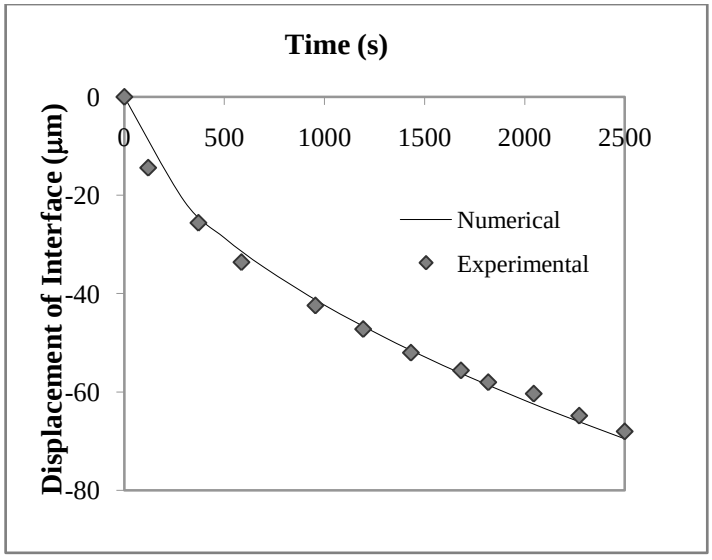

Figure 6.3. Comparing experimental data and numerical results for methanol-air system at ambient pressure

6.3. INTERPHASE DIFFUSION IN CARBON DIOXIDE-EXPANDED LIQUIDS

The diffusion in two different ionic liquids-carbon dioxide and methanol-carbon dioxide binary systems at high pressures is examined. In the case of [bmim][PF_6] and methanol, infinite dilution diffusivities at ambient pressure taken from literature are corrected to the desired pressure using the viscosity data. This correction could not be performed for [thtdp][Cl] as the high pressure viscosity data for this ionic liquid were not available in the literature. The calculations were repeated for the methanol-carbon dioxide system using the composition-dependent diffusivities determined based on the Maxwell-Stefan Theory.

6.3.1. Carbon Dioxide-Ionic Liquid Systems At High Pressure

The interphase diffusion in these systems is investigated at a pressure of 75 bar and a temperature of 313 K. Since the pressure is high, the gas is soluble in the liquid phase while the transport of ionic liquids into the vapor phase is negligible [46]. In other words, there is one-way mass transfer in the system; only from vapor to liquid phase.

Figure 6.4 indicates the displacement of the phase interface with time in the [bmim][PF_6]-carbon dioxide system. Due to the diffusion, the amount of liquid phase increases in the capillary; the interface moves up about 0.67 mm in 2500 s. At the beginning, the movement of the interface is faster because of the large concentration gradient at the interface. Eventually, the dissolution rate reaches a constant value.

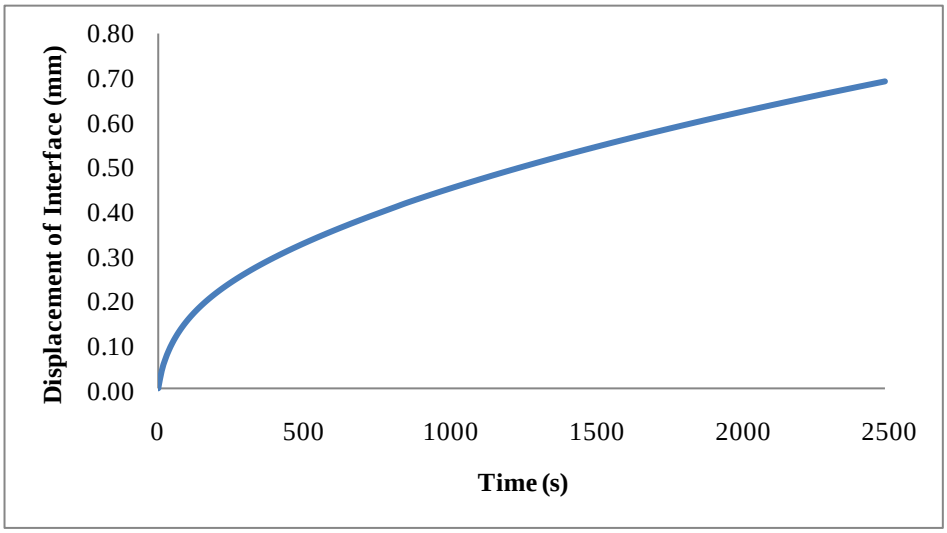

Figure 6.4. Interface Displacement of [bmim][PF_6]-CO_2 system at 75 bars and 313.14 K

Figure 6.5 shows the composition profiles of carbon dioxide and [bmim][PF_6] at 2500 seconds. Since the liquid is not soluble in the gas phase, the mole fraction of carbon dioxide stays constant at one here. At the interface, the mole fraction of carbon dioxide is constant at 0.51 (see Table 1) and decreases to zero in the bulk of the ionic liquid. The dissolution rate would be further reduced as the concentration front begins to approach to the bottom of the tube.

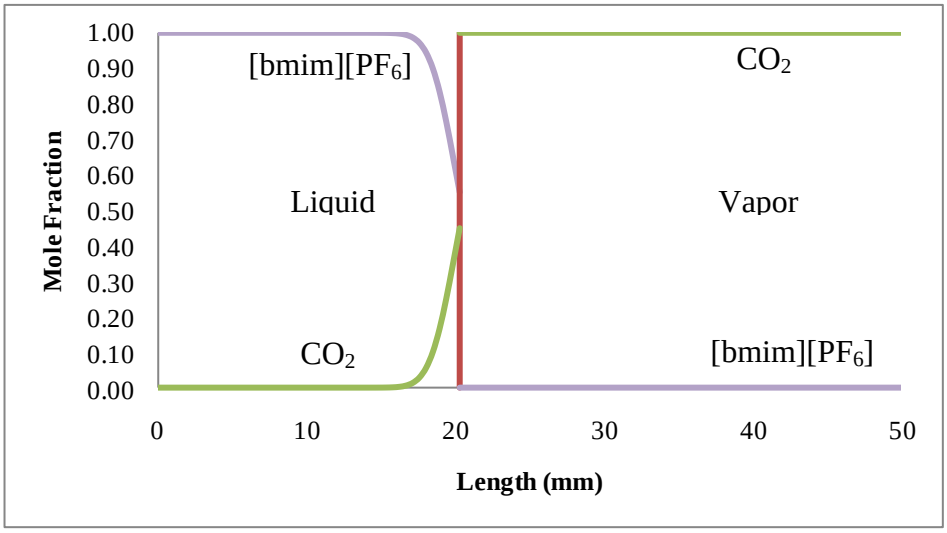

Figure 6.5. Composition profiles of [bmim][PF_6]-CO_2 system at t=2500 s

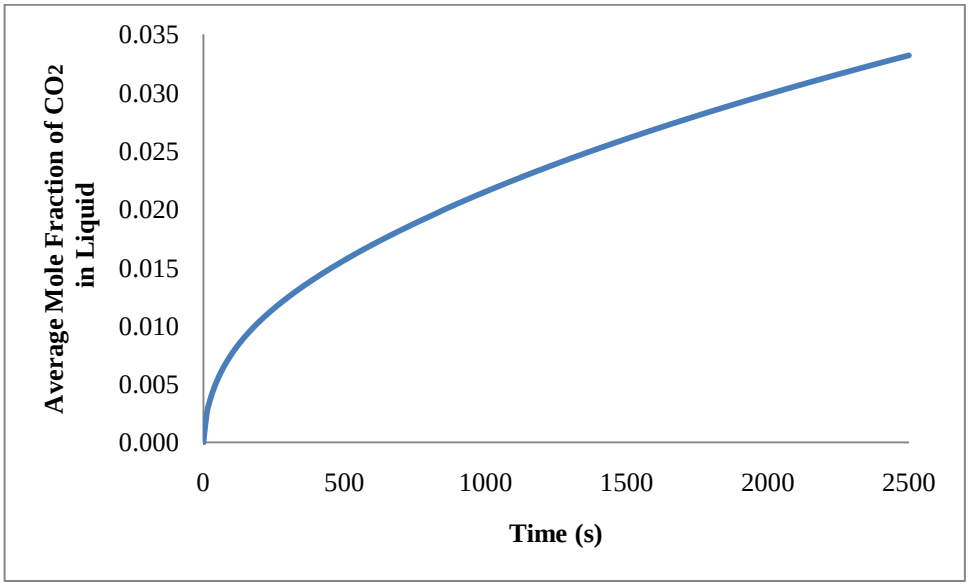

Figure 6.6. Average Mole fraction of CO_2 in liquid phase in [bmim][PF_6]-CO_2 system for t=2500 s

Figure 6.6. shows the average mole fractions of CO_2 in liquid phase in [bmim][PF_6]-CO_2 system in the same time period as before. Initially, the mole fraction of CO_2 in the liquid phase has been zero. As the diffusion process takes place the mole fraction of CO_2 in liquid phase starts to increase. From the experimental data presented in Table 6.1. [61], the

equilibrium fraction is 0.51. At t=2500 seconds the average mole fraction of CO_2 is 0.032, which indicates that the system is still far from equilibrium.

Table 6.1. Equilibrium mole fractions of CO_2 and [bmim][PF_6] at 313.15 K and 75 bar [61]

x_{CO_2}	$x_{[bmim][PF6]}$	y_{CO_2}	$y_{[bmim][PF6]}$
0.51	0.49	1.0	0.0

We obtained similar results in the case of [thtdp][Cl]–carbon dioxide system. Again, the liquid does not evaporate into the gas phase but expands during the process (see Figure 6.7). The interface moves up about 0.92 mm in 2500 seconds. The interface movement is slightly higher compared to the previous case, since the solubility of carbon dioxide is higher in this ionic liquid.

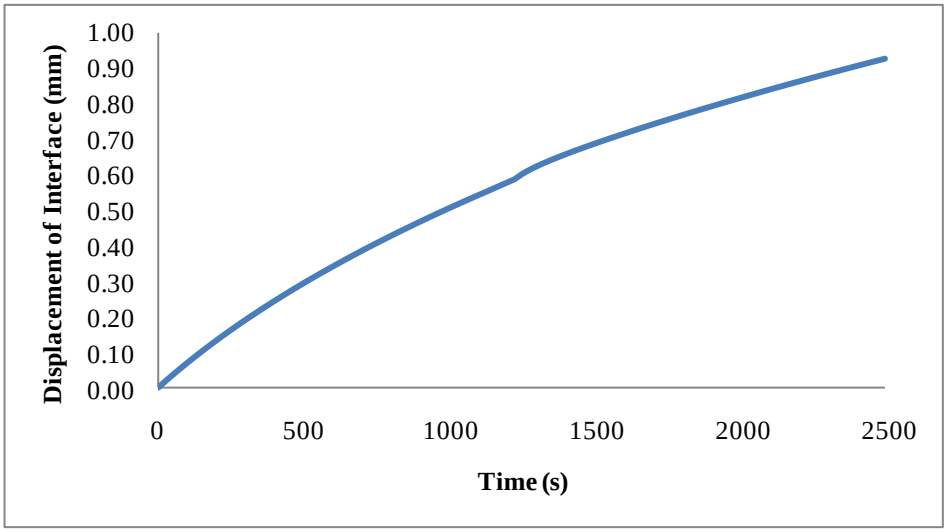

Figure 6.7. Interface Displacement of [thtdp][Cl]-CO_2 system at 75 bars and 313.14 K

The composition profiles at t=2500 seconds is shown in Figure 6.8. In the vapor phase the mole fraction of CO_2 and [thtdp][Cl] are one and zero respectively as no diffusion of ionic liquid into the vapor phase takes place. At the phase boundary the fraction of CO_2 is 0.75 (see Table 6.2) [62]. The concentration front did not reach the bottom of the tube in this case either.

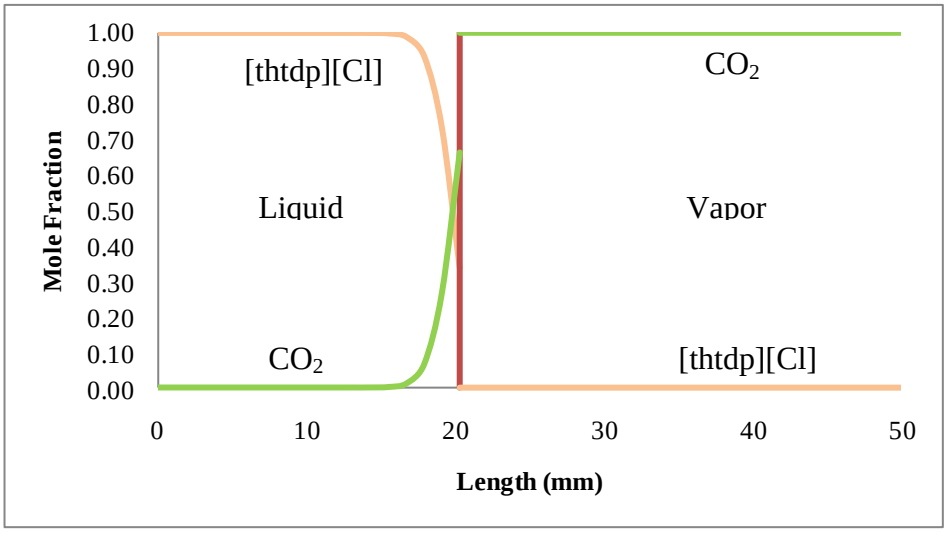

Figure 6.8. Composition profiles of [thtdp][Cl]-CO_2 system at t=2500 s

Figure 6.9. shows the average mole fraction of CO_2 in the liquid phase in [thtdp][Cl]- At t=2500 seconds the average mole fraction of CO_2 is 0.052, still the liquid mixture is dilute in carbon dioxide (see Table 6.2 for equilibrium mole fractions)

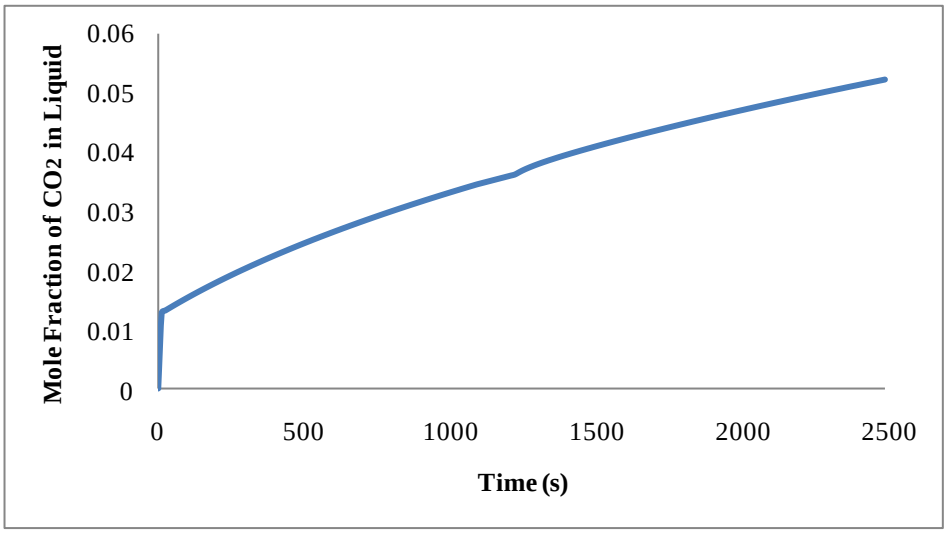

Figure 6.9. Average Mole fraction of CO_2 in liquid phase in [thtdp][Cl]-CO_2 system for t=2500 s

Table 6.2. Equilibrium mole fractions of CO_2 and [thtdp][Cl] at 313.15 K and 75 bar [62]

x_{CO_2}	$x_{[thtdp][Cl]}$	y_{CO_2}	$y_{[thtdp][Cl]}$
0.752	0.248	1.0	0.0

6.3.2. Carbon Dioxide-Methanol System At High Pressure

The methanol-CO_2 system is studied at 73.9 bars and 313.14 K. In this system, there is two-way mass transfer, the evaporation of methanol into the vapor phase and the simultaneous dissolution of carbon dioxide in the liquid phase. First, the calculations are carried out using the pressure-corrected infinite dilution diffusivities.

Figure 6.10 shows the movement of the interface with time. We observe that the dissolution process dominates the vaporization process; the liquid is expanded by carbon dioxide in this case, too. The interface moves up about 3.4 mm in 2500 s and its velocity is higher than those in the ionic liquid-carbon dioxide systems (see Figures 6.4 and 6.7). This result is attributable to the diffusivities. The infinite dilution diffusivity of carbon dioxide in methanol is about twenty times higher than those in the ionic liquids.

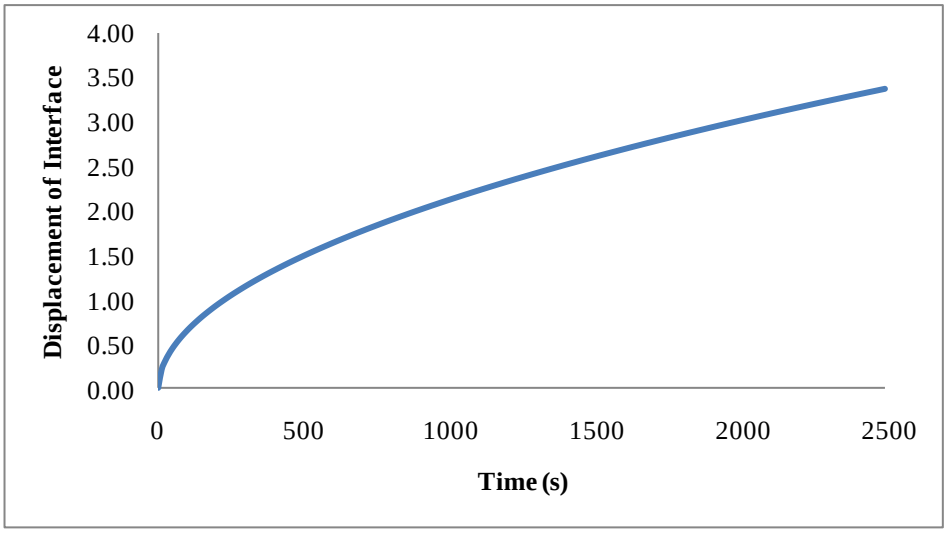

Figure 6.10. Interface Displacement of Methanol-CO_2 system at 73.9 bars and 313.14 K

The composition profiles at t=2500 seconds up to 50 mm of the capillary are shown in Figure 6.11. The mole fraction of CO_2 is constant and equals to 0.59 (see Table 6.3) at the phase interface. It drops to zero in the bulk of the liquid phase. Similarly, in the bulk of the vapor phase the mole fraction of methanol decreases to zero. We also observe that compared to the other systems, the dissolution front has moved faster.

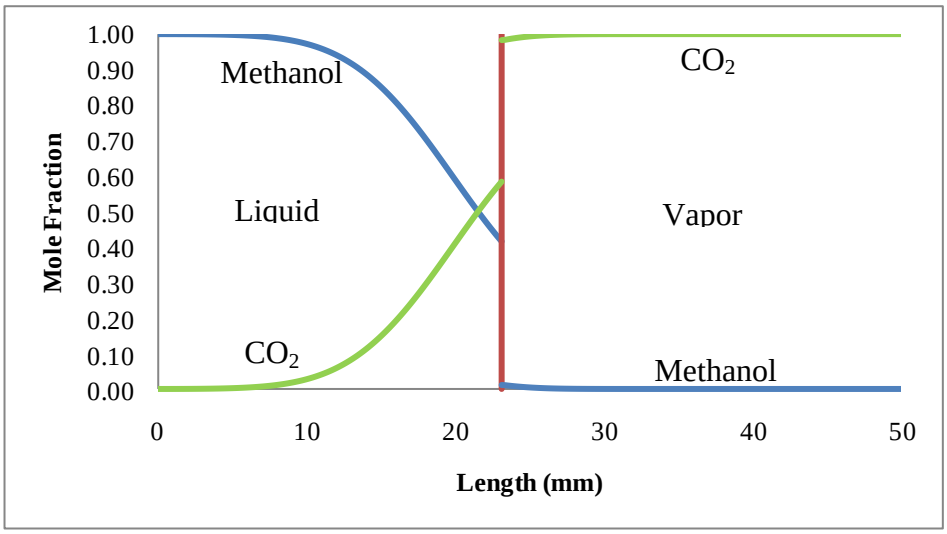

Figure 6.11. Composition profiles of methanol-CO_2 system at t=2500 s

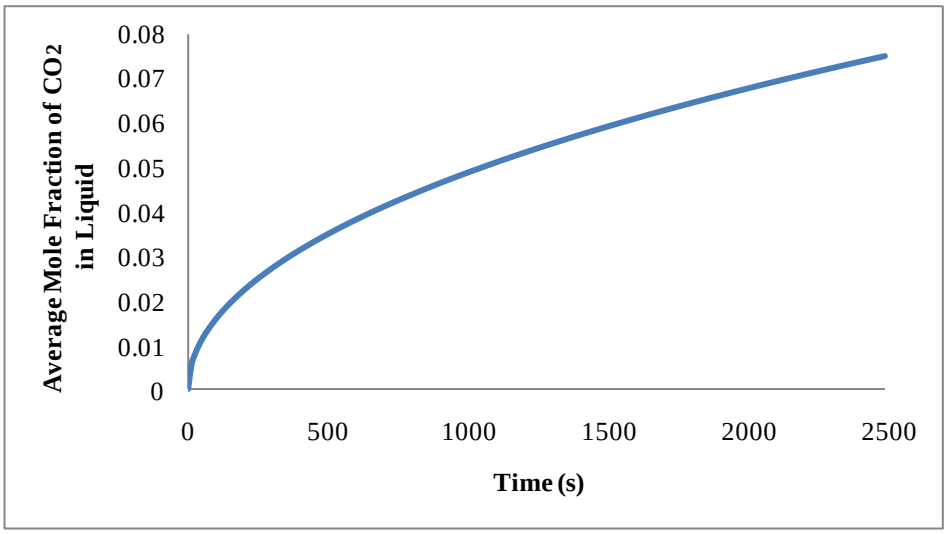

Figure 6.12. Average Mole fraction of CO_2 in liquid phase in Methanol-CO_2 system for t=2500 s

In Figure 6.12 average mole fractions of CO_2 in liquid phase in methanol-CO_2 system is shown. From the experimental data reported by Chang and Day [58] (see Table 6.3) the equilibrium mole fraction of CO_2 in the liquid phase is known to be 0.59. At t=2500 seconds, the average mole fraction of CO_2 is 0.075, higher than those reached by carbon dioxide in the ionic liquids.

Table 6.3. Equilibrium mole fractions of CO_2 and methanol at 313.14 K and 73.9 bar [58]

x_{CO_2}	$x_{methanol}$	y_{CO_2}	$y_{methanol}$
0.5907	0.4093	0.9864	0.0136

The calculations for this system are repeated using the composition dependent diffusivities determined based on the Maxwell-Stefan theory of diffusion. The composition-dependent Maxwell-Stefan diffusivities are calculated using the Vignes formula as explained in Section 5. As CO_2 diffuses into the liquid phase, the diffusivity increases as shown in Figure 6.13.

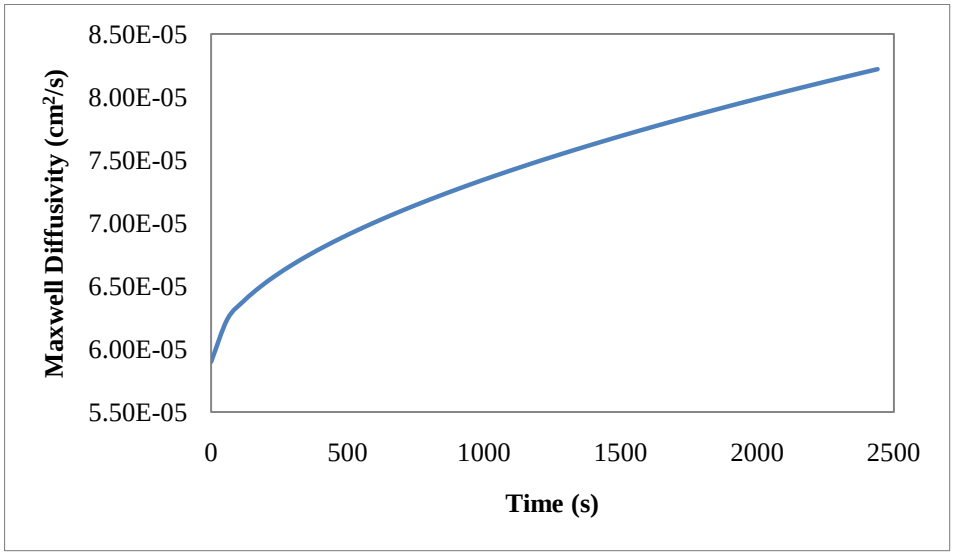

Figure 6.13. Change in Maxwell-Stefan diffusity of Methanol-CO_2 system at 73.9 bars and 313.14 K

On the other hand, the thermodynamic correction factor decreases as the mole fraction of CO_2 in the liquid phase increases (see Figure 6.14).

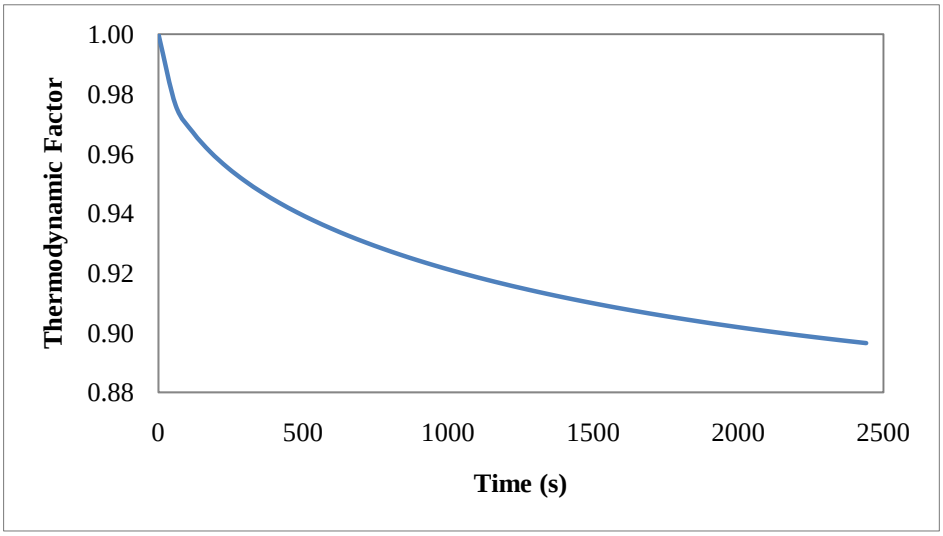

Figure 6.14. Change in thermodynamic factor of Methanol-CO_2 system at 73.9 bars and 313.14 K

The Fick diffusivity is the product of Maxwell-Stefan diffusion coefficients and the thermodynamic correction factors. As expected, the Fick diffusivities are directly proportional to the CO_2 fraction in the liquid phase as presented (see Figure 6.15).

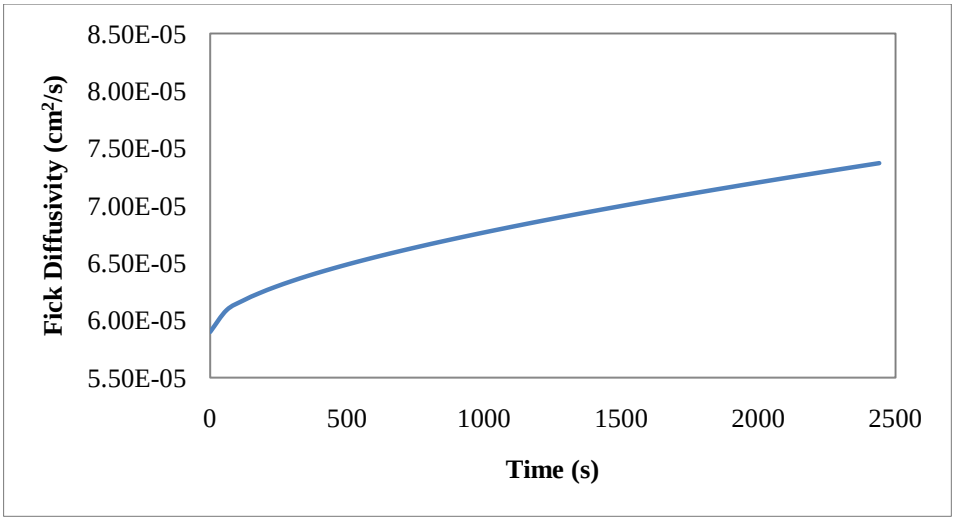

Figure 6.15. Change in Fick diffusivity of Methanol-CO_2 system at 73.9 bars and 313.14 K

The displacement of interface is affected by the diffusivities used. With infinite dilution diffusivities which are pressure corrected, the interface moves up approximately 3.4 mm at t=2500 seconds (see Figure 6.10). However the interface moves up 5.2 mm with

Fick diffusivities for same time interval (see Figure 6.16). As expected increasing diffusivity of CO_2 in methanol, which means higher dissolution rate in liquid, increases the displacement of the interface.

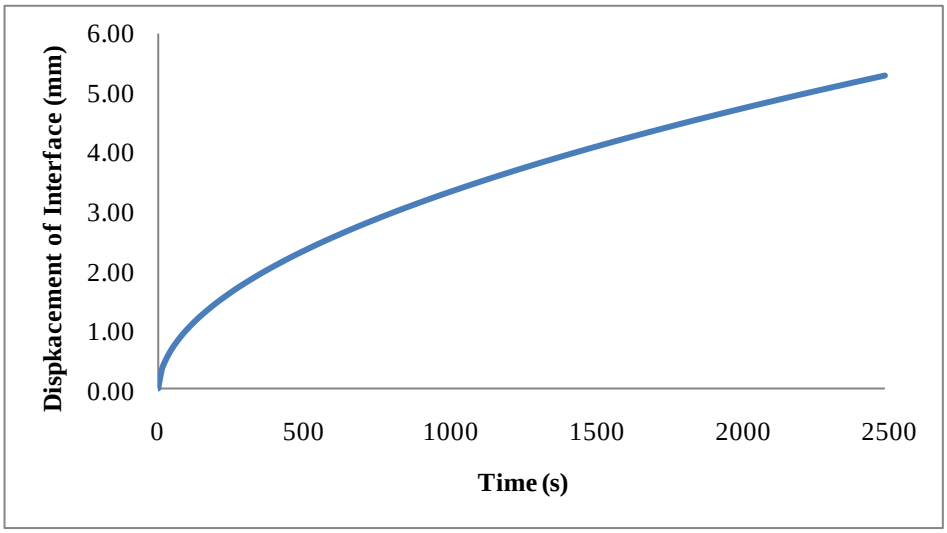

Figure 6.16. Interface Displacement of Methanol-CO_2 system at 73.9 bars and 313.14 K with Fick Diffusivities

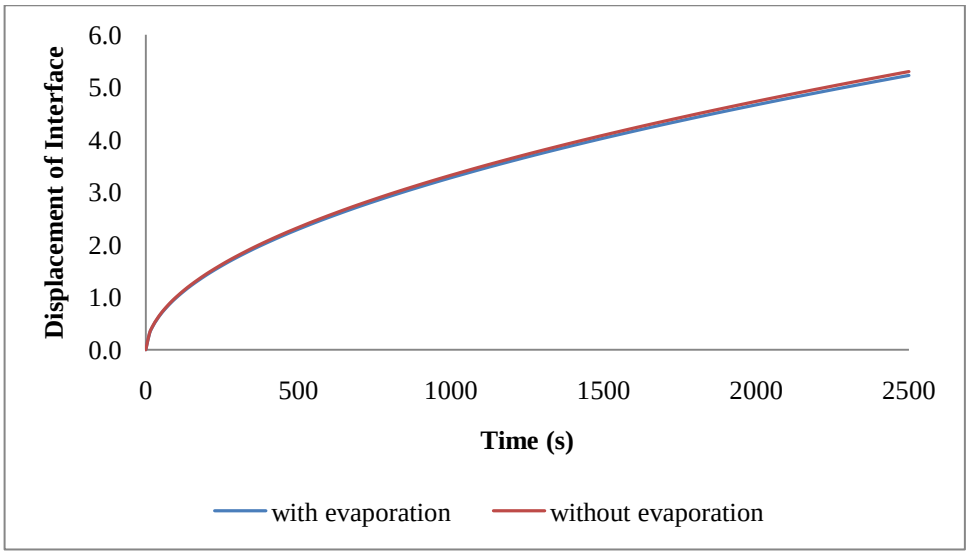

Figure 6.17. Interface Displacement of Methanol-CO_2 system at 73.9 bars and 313.14 K with evaporation and without evaporation

We also compare the dissolution rates to the evaporation rates. As shown in Figure 6.17, the vaporization process is negligible at 313 K and 73.9 bar as far as the displacement of the interface is concerned.

7. CONCLUSIONS AND FUTURE WORK

In this study, we have developed numerical solution programs based on the finite difference formulation that can be applied to moving boundary problems that involve phase change in binary systems (see Appendix A). The method was applied to the evaporation of methanol into air at ambient pressure and the results obtained were comparable to the experimental data.

The numerical solution technique is improved to handle binary systems at high pressure that involve the dissolution of the gas in liquid as well. The diffusion of carbon dioxide into different liquids, namely, two ionic liquids which are [bmim][PF_6] and [thtdp][Cl], and methanol at high pressure is invesigated. In the case of ionic liquids, there is only one-way mass transfer. Due to the dissolution of carbon dioxide in the ionic liquids, the volume of the liquid phase expands. Interface displacements determined for the aforementioned ionic liquids are found to be of the same order of magnitude.

In the methanol-carbon dioxide system, there is two-way mass transfer, the evaporation of methanol into the vapor and the dissolution of carbon dioxide in the liquid. We found that the vaporization rate is lower than the dissolution rate and again a gas-expanded liquid system forms. Compared to the ionic liquid-carbon dioxide systems, the velocity of the phase interface is higher in the case of methanol.

The effect of composition-dependent diffusivity on the interface velocity is also investigated for the methanol-carbon dioxide system. The Fick diffusivity is determined based on the Maxwell-Stefan formulation. As carbon dioxide dissolves in the liquid, Fick diffusivity and therefore, the velocity of the interface increases. As a future work, Maxwell-Stefan formulation will be applied to the ionic liquid-carbon dioxide systems, too. One of the reasons of expanding ionic liquids with carbon dioxide is to improve their transport properties. The enhancement needs to be quantitatively determined in order to design chemical processes involving extraction, reaction operations using these fluid systems.

As another future work, the model will be improved to include the effect of the change in the density of the liquid phase. For this purpose, a thermodynamic model needs to be integrated to the transport model and at every time step, the new mole fractions must be calculated through solving these models simultaneously. Since the equilibrium mole fractions of carbon dioxide in these liquids is on the order of 0.5, we expect that results would get affected especially in the long run.

APPENDIX A : FLOWCHARTS OF FORTRAN PROGRAMS DEVELOPED

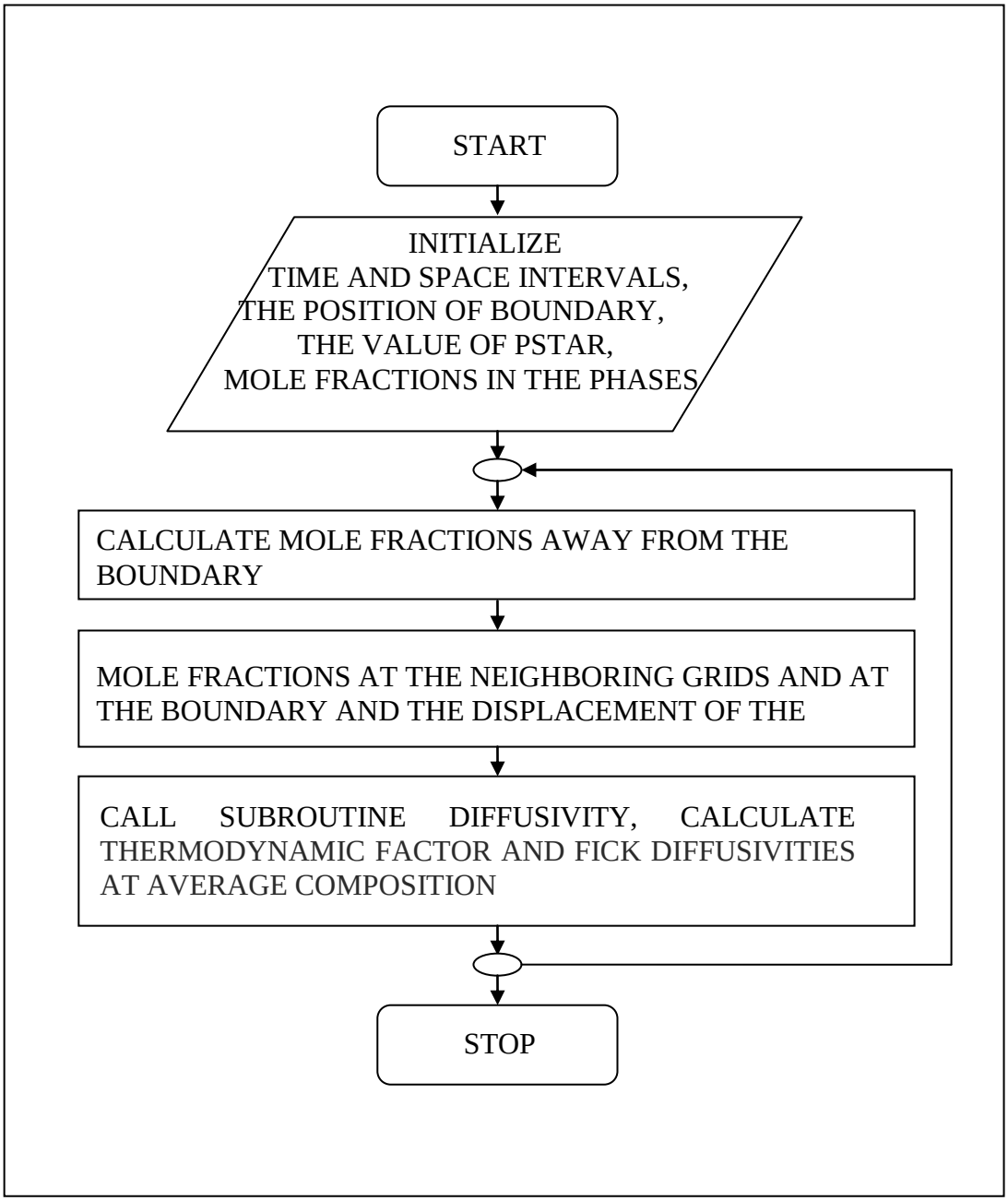

Figure A.1. Flowchart of the main program

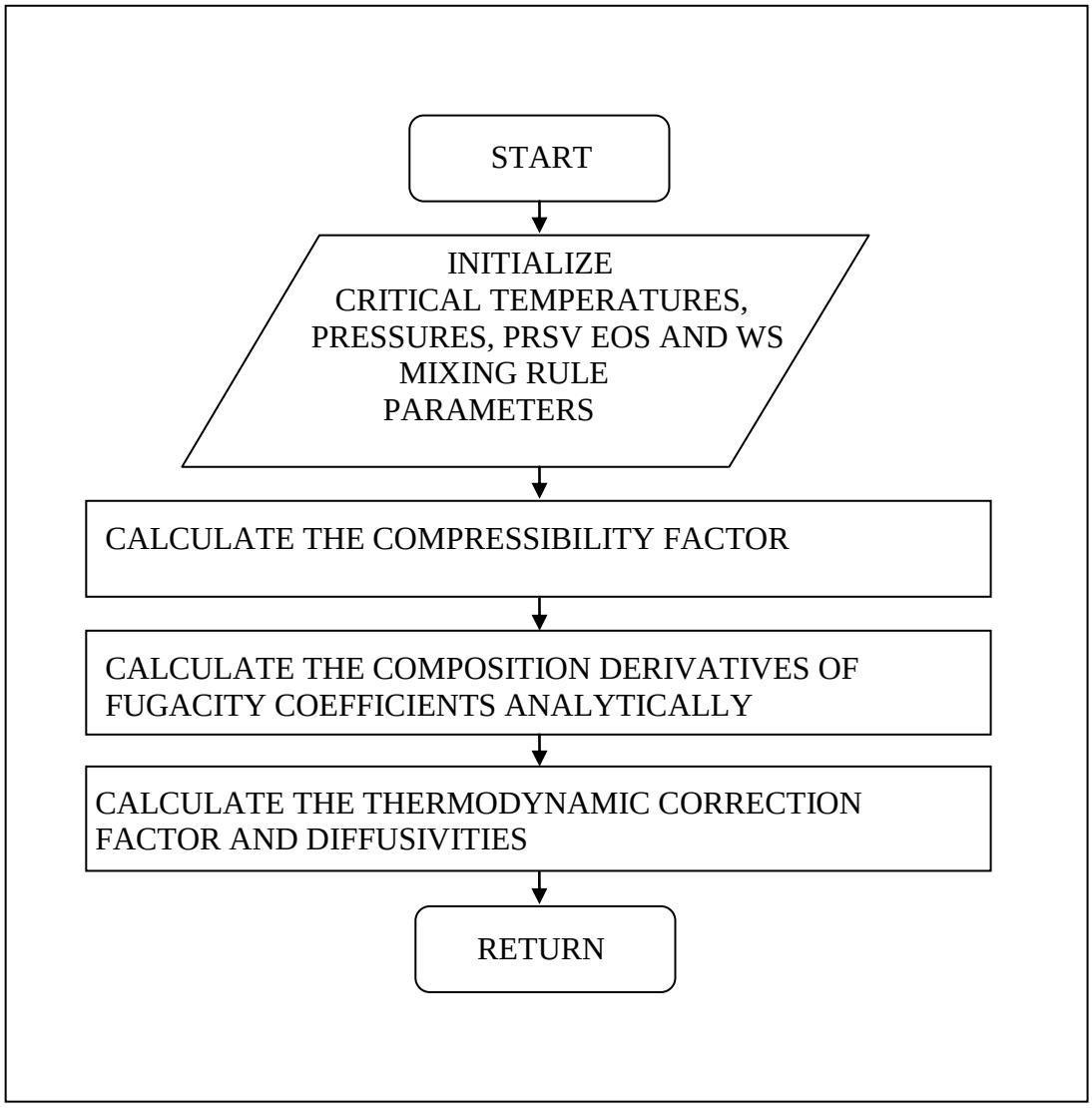

Figure A.2. Flowchart of the subroutine ‘Diffusivity’

APPENDIX B : VISCOSITY DATA

Table B.1. Viscosity of methanol at high pressure [63]

T, °C	Pressure, kg cm^{-2}					
	atm	50.0	100.0	150.0	200.0	250.0
20.0	0.588	0.600	0.615	0.626	0.640	0.656
40.0	0.450	0.462	0.475	0.485	0.498	0.506
60.0	0.350	0.362	0.370	0.380	0.390	0.400
80.0	0.275	0.285	0.292	0.298	0.308	0.316
100.0	0.218	0.226	0.234	0.238	0.246	0.254
120.0	0.174	0.182	0.190	0.194	0.200	0.206
140.0	0.142	0.152	0.158	0.164	0.170	0.174
160.0	---	0.132	0.138	0.145	0.152	0.158

Table B.2. Viscosity of [bmim][PF_6] at high pressure [64]

Temperature, K	Pressure, bar	η (mPa s)
293.15	1.0	382
	50.0	409
	100.0	442
	150.0	468
	200.0	504
313.15	1.0	119
	50.0	126
	100.0	133
	150.0	140
	200.0	151

APPENDIX C : ESTIMATED PARAMETERS FOR METHANOL-CO_2 SYSTEM

Table C.1. Estimated Parameters for Methanol-CO_2 System at 313.14 K [58]

x-exp	y-exp	y-cal	P-exp	P-cal
0.0682	0.9646	0.97057	13.2	13.641
0.0911	0.9727	0.97647	16.7	17.743
0.1159	0.9815	0.98021	20.3	21.997
0.1372	0.9843	0.98230	24.7	25.505
0.1773	0.9849	0.98490	31.3	31.762
0.2006	0.9857	0.98570	36.1	35.202
0.2318	0.9867	0.98670	39.6	39.597
0.2733	0.9876	0.98760	45.6	45.089
0.3464	0.9881	0.98810	55.0	53.844
0.3838	0.9879	0.98790	59.1	57.889
0.4128	0.9882	0.98820	62.0	60.825
0.4658	0.9871	0.98710	66.0	65.728
0.5138	0.9865	0.98650	69.0	69.622
0.5467	0.9867	0.98670	70.6	71.961
0.5907	0.9864	0.98640	73.9	74.633
0.6816	0.9842	0.98420	76.9	78.238
0.8783	0.9677	0.96770	80.3	79.944

ALPHA= 0.3000

K12= 0.3972

NRTL A12= 101.3090 cal/mole

NRTL A21= 426.9296 cal/mole

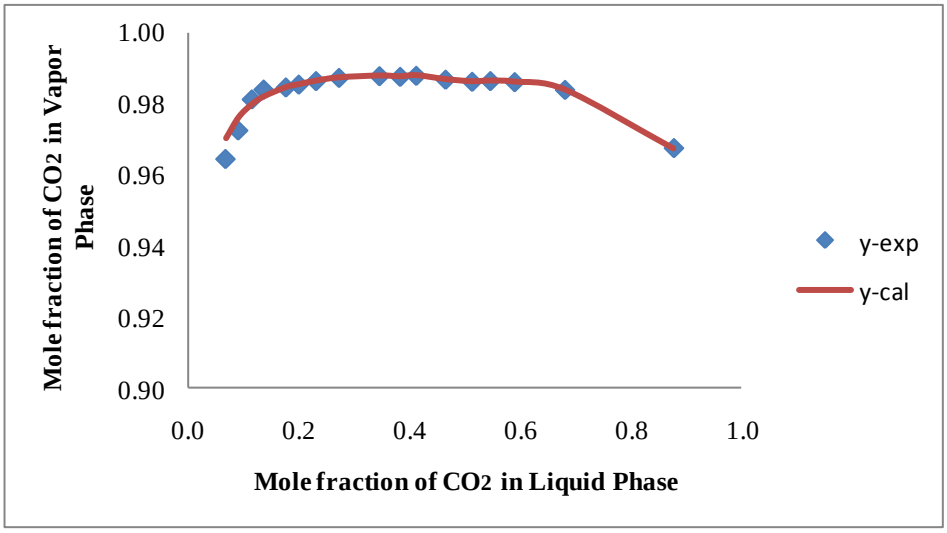

Figure C.1. Calculated and experimental vapor mole fractions for Methanol-CO_2 system

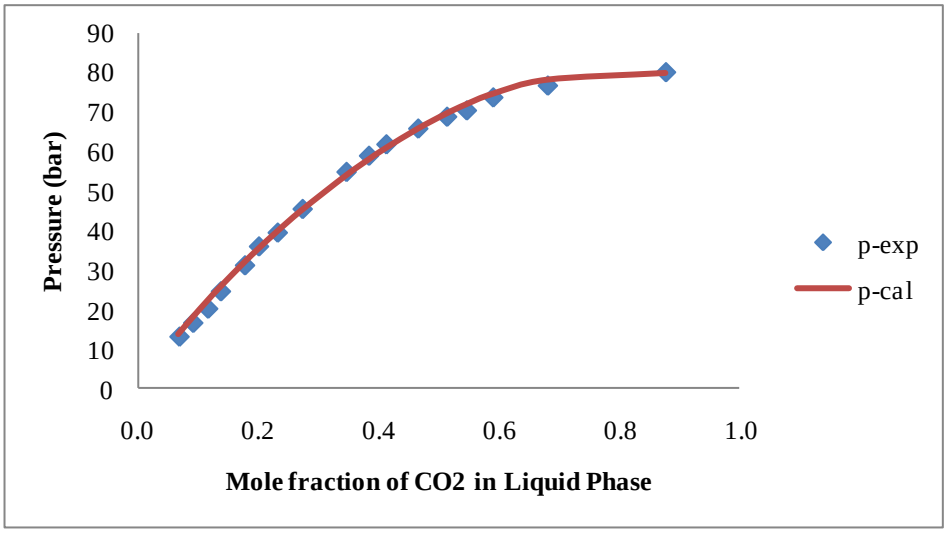

Figure C.2. Calculated and experimental pressures for Methanol-CO_2 system

REFERENCES

1. Williams J. R., and A. A. Clifford, *Supercritical Fluid Methods and Protocols*, Humana Press Inc., USA, 2000.

2. Jessop P. G. and B. Subramaniam, "Gas Expanded Liquids", *Chemical Reviews*, Vol. 107, pp. 2666-2694, 2007.

3. Orbey H., and S. Sandler, *Modeling Vapor-Liquid Equilibria*, Cambridge University Press, USA, 1998.

4. Proust P., and J. H. Vera, "PRSV: The stryjek-vera modification of the Peng-Robinson equation of state. Parameters for other pure compounds of industrial interest", *The Canadian Journal of Chemical Engineering*, Vol. 67, pp. 170-173, 1989.

5. Henderson D., and J. P. Leonard, "One- and Two-Fluid van der Waals Theories of Liquid Mixtures, II. 6:12 Molecules", *Proceedings of the National Academy of Sciences*, Vol. 68, pp. 632-635, 1971.

6. Johnston K. P., S. R. Rocha, C. T. Lee, and M. Z. Yates, "Colloid and Interface Science for Carbon Dioxide-Based Pharmaceutical Processes", *Supercritical Fluid Technology for Drug Development*, Marcell Dekkar Inc., New York, 2004.

7. Jessop G. P., and W. Leitner, *Chemical Synthesis Using Supercritical Fluids*, Wiley-VCH, Germany, 1999.

8. Environmental Protection Agency, Supercritical CO_2 as a Solvent Media, www.epa.gov/nrmrl/std/cppb/greenchem/greenchemscco2.htm, 2010.

9. Phelps M. R., M. O. Hogan, and L. J. Snowden-Swan, *Waste Reduction Using*

Carbon Dioxide: A Solvent Substitute For Precision Cleaning Applications, Precision Cleaning '95 Proceedings, USA, 1995.

10. M. Bouchaour, N. Diaf, A. Ould-Abbas, M. Benosman, L. Merad and N-E. Chabane-Sari, "The Role of Supercritical CO_2 in the Drying of Porous Silicon", Renewable Energy Reviews, Vol. 29, pp. 99-102, 2003.

11. Foster N. R., H. Singh, S.L.J. Yun, D.L. Tomasko, and S.J. Macnaughton, "Polar and nonpolar cosolvent effects on the solubility of cholesterol in supercritical fluids", *Industry & Engineering Chemistry Research*, Vol. 32, pp. 2849-2853, 1993.

12. Ekart M. P., K.L. Bennett, S.M. Ekart, G.S. Gurdial, C.L. Liotta, and C.A. Eckert, "Cosolvent interactions in supercritical fluid solutions", *American Institute of Chemical Engineers Journal*, Vol. 39, pp. 235-248, 1993.

13. Brinker C. J., and G. W. Scherer, *Sol-Gel Science: The Physics and Chemistry of Sol-Gel Processing*, Academic Press, USA, 1989.

14. St Andrews University's School of Chemistry, Conservation of Artefacts by Supercritical Drying, http://ch-www.st-andrews.ac.uk/wood/SCD.html, 1998.

15. Steiner S., Properties of Aerogels, www.aerogel.org, 2008.

16. Hench, L.N., and J.K. West, "The Sol-Gel Process", *Chemical Reviews*, Vol. 90, pp. 33-72, 1990.

17. Buckley A. M., and M. Greenblatt, "The Sol-Gel Preparation of Silica Gels", *Journal of Chemical Education*, Vol. 71, pp. 599-602, 1994.

18. Mukhopadhyay M., and B. S. Rao, "Modeling of supercritical drying of ethanol-soaked silica aerogels with carbon dioxide", *Journal of Chemical Technology and Biotechnology*, Vol. 83, pp. 1101-1109, 2008.

19. Hutchenson K. W., A. M. Scurto and B. Subramaniam, *Gas-Expanded Liquids and Near-Critical Media*, American Chemical Society, USA, 2009.

20. Jessop P.G., R.R. Stanley, R.A. Brown, C.A. Eckert, C.L. Liotta, and T.T. Ngo, "Neoteric solvents for asymmetric hydrogenation: supercritical fluids, ionic liquids, and expanded ionic liquids", *Green Chemistry*, Vol. 5, pp. 123, 2003.

21. Yoon J., H. S. Lee and H. Lee, "High-pressure vapor-liquid equilibria for carbon dioxide + methanol, carbon dioxide + ethanol, and carbon dioxide + methanol + ethanol", *Journal of Chemical Engineering Data*, Vol. 38, pp. 53-55, 1993.

22. Blanchard L., Z. Gu, and J. Brennecke, "High-pressure phase behavior of ionic liquid/CO_2 systems", *Journal of Physical Chemistry B*, Vol. 105, pp. 2437-2444, 2001.

23. Warwick B., F. Dehghani, N. R. Foster, J. R. Biffin, and H. L. Regtop, "Micronization of copper indomethacin using gas antisolvent processes", *Industry & Engineering Chemical Research*, Vol. 39, pp. 4571-4576, 2000.

24. Blanchard L. A., J. F., "Brennecke Esterification of acetic acid with ethanol in carbon dioxide", *Green Chemistry*, Vol. 3, pp. 17-19, 2001.

25. Combes G. B., F. Dehghani, F. P. Lucien, A. K. Dillow, and N. R. Foster, "Asymmetric catalytic hydrogenation in CO_2 expanded methanol an application of gas antisolvent reactions (GASR)", *Reaction engineering for pollution prevention*, Elsevier, 1999.

26. Baiker A., "Supercritical Fluids in Heterogeneous Catalysis", *Chemical Reviews*, Vol. 99, pp. 453-474, 1999.

27. Cleve E., E. Bach, and E. Schollmeyer, "Untersuchungen zum Schmelz- und Strukturverhalten von Polyethylenterephthalatfasern in Luft bei 1 bar und in überkritischem CO_2 bis 280 bar", *Die Angewandte Makromolekulare Chemie*, Vol.

256, pp. 39-48, 1998.

28. Takada M., and M. Ohshima, **“** Effect of CO_2 on crystallization kinetics of polyethylene terephthalate”, *Polymer Engineering Science,* Vol. 43, pp. 479-484, 2003.

29. Jung J., and M. J. Perrut, “Particle design using supercritical fluids: Literature and patent survey”, *Journal of Supercritical Fluids,* Vol. 20, pp. 179-188, 2001.

30. Yeo S., and E. Kiran, “Formation of Polymer Particles with Supercritical Fluids: A Review”, *Journal of Supercritical Fluids,*Vol. 34, pp. 287-292, 2005.

31. Pourmortazavi S. M., and S. S. Hajimirsadeghi, “Application of supercritical carbon dioxide in energetic materials processes: A review”, *Industrial & Engineering Chemistry Research,* Vol.44, pp. 6523-6533, 2005.

32. Shishikura A., K. Kanamori, H. Takahashi, and H. Kinbara, “Separation and purification of Organic Acids by Gas Anti-Solvent Crystallisation”, *Journal of Agricultural and Food Chemistry*, Vol. 42, pp. 1993-2003, 1994.

33. Chang, C. J., and A. D. Randolph, “Separation of β-Carotene Mixtures Precipitated from Liquid Solvents with High-Pressure CO_2”, *Biotechnology Progress,* Vol. 7, pp. 275-287, 1991.

34. Kirchner B., *Ionic Liquids*, Springer, Berlin, 2009.

35. Keskin S., Defne K.T., Uğur A., and Ömer H., “A Review of Ionic Liquids Toward Supercritical Fluid Applications”, *Journal of Supercritical Fluids,* Vol. 43, pp. 150-180, 2007.

36. Reddy R. G., “Ionic Liquids: How Well Do We Know Them?”, *Journal of Phase Equilibria and Diffusion*, Vol. 27, pp. 210-211, 2006.

37. Huddleston J.G., H.D.Willauer, R.P. Swatloski, A.E.Visser, and R.D. Rogers, "Room temperature ionic liquids as novel media for clean liquid–liquid extraction", *Chemical Community*, Vol. 3, pp. 1765–1766, 1998.

38. Dai S., D. DePaoli, M. Dietz, J. Mays, J. McFarlane, and W. Steele, "Technical summaries on ionic liquids in chemical processing", *Chemical Industry Vision 2020 Technology Partnership Workshop*, 2003.

39. Morland R., "American Chemical Society Division of Industrial and Engineering Chemistry", *Proceedings of the 221st American Chemical Society National Meeting*, San Diego, 2001.

40. Zhao H., S. Xia, and P. Ma, "Use of ionic liquids as green solvents for extractions", *Journal of Chemical Technology and Biotechnology*, Vol. 80, pp. 1089-1096, 2005.

41. Aki S.N., B.R. Mellein, E.M. Saurer, and J.F. Brennecke, "High-pressure phase behavior of carbon dioxide with imidazolium-based ionic liquids", *Journal of Physical Chemistry B*, Vol. 108, pp. 20355-20365, 2004.

42. Crank J., *The Mathematics of Diffusion*, 2nd edition, Oxford University Press, New York, 1975.

43. Shewmon P., *Diffusion in Solids*, McGraw-Hill, New York, 1963.

44. Mehrer H., *Diffusion in Solids*, Springer, Berlin, 2007.

45. Maxwell J. C., "On the dynamical theory of gases", *The Scientific Papers of J. C. Maxwell*, Vol. 2, pp. 26-78, 1965.

46. Bosse D., *Diffusion, Viscosity, and Thermodynamics in Liquid Systems*, PhD Thesis, Technischen Universitat Kaiserslautern, Germany, 2005.

47. Vuik C., *Some Historical Notes On The Stefan Problem*, Delft University of

Technology, Netherlands, 2003.

48. Crusius S., G. Inden, U. Knoop, L. Höglund, and J. Agren, "On the Numerical Treatment of Moving Boundary Problems", *Zeitschrift für Metallkunde*, Vol. 83, pp. 673-678, 1992.

49. Crank J., *Free and Moving Boundary Problems*, Oxford University Press Inc., New York, 1984.

50. Zhou, Y., T.H. North, "Kinetic modelling of diffusion-controlled, two-phase moving interface problems", *Modelling and Simulation in Materials Science and Engineering*, Vol. 1, pp. 505, 1993.

51. Crank J., *The Mathematics Of Diffusion*, Clarendon Press, Oxford, 1975.

52. Lee B.J., K.H. Oh, "Numerical treatment of the moving interface in diffusional reactions", *Zeitschrift Fur Metallkunde*, Vol. 87, pp. 195–204, 1996.

53. Renon H., Prausnitz J. M., "Local Compositions in Thermodynamic Excess Functions for Liquid Mixtures", *American Institute of Chemical Engineers Journal*, Vol. 14, pp. 135-144, 1968.

54. Kıran E., and L. Sengers, *Supercritical Fluids: Fundamentals and Applications*, Kluwer Academic Publishers, Netherlands, 1994.

55. Kontogeorgis G., and G. M. Folas, *Thermodynamic Models For Industrial Applications: From Classical And Advanced Mixing Rules To Association Theories*, John Wiley & Sons Ltd., Great Britain, 2010.

56. Krishna, R., and Wesselingh, J. A.,"The Maxwell-Stefan Approach to Mass Transfer", *Chemical Engineering Science*, Vol. 52, pp. 861-911, 1997.

57. Matthews, M. A. and A. Akgerman, "Infinite Dilution Diffusion Coefficients of

Methanol and 2-propanol in Water", *Journal of Chemical Engineering Data,* Vol. 33, pp. 122-123, 1988.

58. Chang C. J., C. Y. Day, C. M. Ko, and K. L. Chiu, "Densities And P-x-y Diagrams for Carbondioxide Dissolution in Methanol, Ethanol, and Acetone Mixtures", *Fluid Phase Equilibria,* Vol. 131, pp. 243-258, 1997.

59. He C., and Y. Yu, "New Equation for Infinite-Dilution Diffusion Coefficients in Supercritical and High-temperature Liquid Solvents", *Industrial Engineering and Chemical Research,* Vol. 37, pp. 3793-3798, 1998.

60. Slattery J. C., and V. R. Mhetar, "Unsteady-state evaporation and the measurement of a binary diffusion coefficient", *Chemical Engineering Science,* Vol. 52, pp. 1511-1515, 1997.

61. Morgan D., L. Ferguson, and P. Scovazzo, "Diffusivities of Gases in Room-Temperature Ionic Liquids: Data and Correlations Obtained Using a Lag-Time Technique", *Industry & Engineering Chemistry Research,* Vol. 44, pp. 4815-4823, 2005.

62. Carvalho P. J., V. H. Alvarez, I. M. Marrucho, M. Aznar, and A. P., Coutinho, "High carbon dioxide solubilities in trihexyltetradecylphosphonium-based ionic liquids" *The journal of supercritical fluids,* vol 52, pp. 258-265, 2010.

63. Isakova N. P., and L. A. Oshueva, "Viscosity of Liquid Methanol at High Pressures", *Russian Journal of Physical Chemistry,* Vol. 40, pp. 1130-1131, 1966.

64. Tomida D., A. Kumagai, K. Qiao, and C. Yokoyama, "Viscosity of [bmim][PF_6] and [bmim]BF4 at High Pressure", *International Journal of Thermophysics,* Vol. 27, pp. 39-47, 2006.